UNIVERSITAT POLITÈCNICA DE CATALUNYA
BARCELONATECH
Escola d'Enginyeria de Telecomunicació
i Aeroespacial de Castelldefels

TREBALL DE FI DE GRAU

TFG TITLE: CFD study of two-phase flows in hypergravity conditions with OpenFOAM

DEGREE: Grau en Enginyeria de Sistemes Aeroespacials

AUTHOR: Adrià Espinosa Miguel

ADVISOR: Santiago Arias Calderón

DATE: July 12, 2019

Title : CFD study of two-phase flows in hypergravity conditions with OpenFOAM
Author: Adrià Espinosa Miguel

Advisor: Santiago Arias Calderón

Date: July 12, 2019

Overview

Nowadays we are in the greatest space and air era ever, in which technology has been forced to develop up to the point of being applied in gravity conditions that cannot be found on Earth surface. The application of two-phase fluid systems in spacecraft are of great interest to this sector due to its advantages, including: weigh reduction, enhanced performance and efficiency improvement, all of them in comparison with mono-phase fluids. The most remarkable examples where are used biphasic fluids are space bioreactors, chemical gas-liquid contactors, propulsion systems, thermal management systems including fuel or electronics cooling, and spatial life-support systems. Even though the wide variety of technological applications, there are very few hypergravity studies and most of them focus on making spacecraft's components the more resistant as possible. Therefore, the fluid flow research in hypergravity conditions is a very unknown area that requires further investigation.

Some years ago Francesc Suñol and Ricard González-Cinca performed an experimental analysis of the effects of gravity on bubble formation and rise in a low viscosity liquid (distilled-water). This study was carried in the hypergravity environment generated by the large diameter centrifuge of the European Space Agency. So, in the work presented it has been reproduced the mentioned research with a CFD software called OpenFOAM with two main objectives: analyse the same aspects regarding the bubble formation and rise processes, since its behaviour changes as the gravity level increases, and compare the results obtained from the numerical simulations with the previous ones, in order to validate the CFD program for this use.

This project has an important part that consists in validations, where we have studied the most important parameters for the simulations, such as: the contact angle of the fluid and the convergence of the mesh and time step. In addition to the analysis of the transient between two consecutive bubbles, and the bubble formation process in normal gravity and in hypergravity conditions. Then, we performed the final tests to study the bubble rise velocity and volume. The corresponding simulations were set in different hypergravity conditions, for three gas injection velocities: $0.03m/s$, $0.06m/s$ and $0.1m/s$.

Finally, comparing the OpenFOAM results with the ones obtained in the previous research, it can be stated that CFD software can reproduce a fluid flow experiment successfully. The detachment of the bubble from the capillary is determined by surface tensions and buoyancy force, although at higher gravity levels this process is accelerated. Posterior bubble rise follows a zig-zag path that is destabilized and accelerated as gravitational effects increase, which leads to a variation in the oscillation amplitude and frequency, as shown in [1].

Títol: Estudi CFD de fluids bifàsics en condicions d'hipergravetat amb OpenFOAM
Autor: Adrià Espinosa Miguel

Director: Santiago Arias Calderón

Data: 12 de juliol de 2019

Resum

Avui en dia ens trobem a l'època més important de l'espai i de l'aire, lo qual ha portat a que la tecnologia s'hagi vist obligada a desenvolupar-se fins al punt de poder ser utilitzada en condicions gravitacionals que no es troben a la superfície de la Terra. L'aplicació de sistemes de fluids bifàsics en avions, però sobretot en naus espacials és de gran interès per al sector a causa dels seus avantatges, entre els quals destaquen: la reducció de pes, millora del rendiment i millores en l'eficiència dels sistemes, totes elles en comparació amb fluids monofàsics. Els exemples més notables on s'utilitzen els fluids bifàsics són els bioreactors espacials, contactors químics de gas-líquid, sistemes de propulsió, sistemes de gestió tèrmica, incloent el refredament de combustible o electrònica, i els sistemes de suport de vida espacials. Tot i la gran varietat d'aplicacions tecnològiques, hi ha molt pocs estudis en condicions d'hipergravetat i la majoria d'ells es centren en fabricar components de naus lo més resistents possible. Per tant, la investigació de flux de fluids en condicions d'hipergravetat és una àrea molt desconeguda que requereix més investigació.

En Francesc Suñol i en Ricard González-Cinca van realitzar fa uns anys un estudi experimental sobre els efectes de la gravetat en la formació de bombolles i el seu ascens dins d'un líquid de baixa viscositat (aigua destil·lada). Aquest estudi es va dur a terme en l'entorn d'hipergravetat artificial generat per la centrifugadora de gran diàmetre de l'Agència Espacial Europea. Així doncs, en aquest TFG s'ha reproduït l'esmentada investigació amb un programa CFD anomenat OpenFOAM i amb dos objectius principals: analitzar els mateixos aspectes relatius a la formació de bombolles i el seu ascens, ja que el seu comportament canvia a mesura que augmenta el nivell de gravetat, i comparar els resultats obtinguts a partir de les simulacions numèriques amb els resultats de l'experiment previ, per tal de validar el programa per aquest ús.

Aquest projecte té una part important que consisteix en validacions, on hem estudiat els paràmetres més importants per a les simulacions, com ara: l'angle de contacte del fluid i la convergència de la malla i del pas de temps. A més de l'anàlisi del transitori entre dues bombolles consecutives, i el procés de formació de bombolles en gravetat normal i en condicions d'hipergravetat. Després d'aquestes validacions es van realitzar les proves finals per mesurar el volum i la velocitat d'ascens de les bombolles. Les simulacions corresponents es van definir en diferents condicions d'hipergravetat, per a tres velocitats de injecció de gas: $0,03m/s$, $0,06m/s$ i $0,1m/s$.

Finalment, comparant els resultats d'OpenFOAM amb els obtinguts de la recerca anterior, es pot afirmar que el programa CFD utilitzat pot reproduir un problema de flux de fluids amb èxit. El despreniment de la bombolla del capil·lar està determinat per les tensions superficials i per la força de flotabilitat, encara que per a valors de gravetat més alts aquest procés s'accelera. El posterior ascens de la bombolla segueix una trajectòria en zig-zag que és desestabilitza i accelera a mesura que els efectes gravitacionals són més grans, el que comporta una variació de l'amplitud i la freqüència de l'oscil·lació, com s'observa en [1].

CONTENTS

List of symbols 1

Acknowledgements 3

Introduction 5

Fluids in altered gravity conditions 8

Rising bubbles 11

CHAPTER 1. Theoretical framework 13

1.1. Contact angle 13

1.2. Dimensionless numbers 14

1.2.1. *Re*, *Bo* and *We* 14

1.2.2. Courant number 15

CHAPTER 2. Problem statement 17

2.1. Background 17

2.1.1. Theoretical framework of the experiment 17

2.1.2. Experiment set-up 18

CHAPTER 3. Methodology of the experiment in OpenFOAM 21

3.1. The software 21

3.2. The case structure 22

3.3. Pre-Processing 23

3.3.1. Geometry of the OpenFOAM's volume 23

3.3.2. The mesh 25

3.3.3. Fluid properties and dimensionless numbers 26

3.3.4. Initial and boundary conditions 27

3.4. Processing 28

3.4.1. InterFoam 28

3.5. Post-Processing 29

3.5.1. Bubble volume . . . 30
3.5.2. Bubble rise velocity . . . 31

CHAPTER 4. Validations . . . 33

4.1. Contact angle tests . . . 33

4.2. Mesh convergence . . . 35

4.3. Time step convergence . . . 38

4.4. Influence of the transient . . . 41

4.5. Bubble formation process . . . 44

CHAPTER 5. Results and Discussion . . . 47

5.1. Path Transition . . . 48

5.2. Analysis of bubble volume and rise velocity . . . 50

Conclusions . . . 55

Bibliography . . . 57

APPENDIX A. OpenFOAM . . . 61

A.1. OpenFOAM case . . . 61
A.1.1. Constant folder . . . 61
A.1.2. System folder . . . 63
A.1.3. 0 folder . . . 70

APPENDIX B. Mesh Generation . . . 73

LIST OF FIGURES

1 Gravity conditions during parabolic flight. 7
2 Flame shape on earth versus in microgravity. 9
3 Bubble formation from a capillary in microgravity conditions. 10
4 ESA's LDC generating high-gravity levels. 12

1.1 Contact angle definition. 13

2.1 Bubble detachment and rise for a steady flow. 18
2.2 Inside of the gondola where the experiment was placed. 18

3.1 OpenFOAM's structure diagram. 22
3.2 Scheme of a general OpenFOAM's folder case structure. 23
3.3 Schematic representation of the bubble stream formation in Suñol and González-Cinca's experiment (left) versus in the virtual experiment (right). 24
3.4 OpenFOAM's geometry frontal and vertical views. 24
3.5 Views of the mesh generated in OpenFOAM by means of the m4 file. 25
3.6 Phase fraction as a function of time for $U_{sg} = 0.06m/s$. 30

4.1 Influence of the contact angle in bubble formation at t=0.05s. 34
4.2 Bubble volume as a function of the number of cells for different gravity levels at $U_{sg} = 0.06m/s$. 36
4.3 Bubble rise velocity as a function of the number of cells for different gravity levels at $U_{sg} = 0.06m/s$. 37
4.4 Bubble volume as a function of the time step for different gravity levels at $U_{sg} = 0.06m/s$. 39
4.5 Bubble rise velocity as a function of the time step for different gravity levels at $U_{sg} = 0.06m/s$. 40
4.6 Capture of the transient event along bubble formation. 41
4.7 Bubble volume and rise velocity for different bubbles of the same simulation. . . 42
4.8 Relative errors in volume and rise velocity results for different gravity levels. . . 43
4.9 Growth and detachment stages of bubble formation. 44
4.10 Outlines of the bubbles during the formation process. 45
4.11 OpenFOAM's bubble formation for 1g and 5g. 46

5.1 Bubble rise comparison between experimental results (1st column) and simulations (2nd column). 47
5.2 Example of bubble trajectory. a) Vertical component of velocity, (b) y position from camera data, (c) x position from camera data, and (d) three-dimensional reconstruction of full trajectory. 48
5.3 Trajectory transition of the bubble regarding U_{sg} for different gravity levels. . . . 49
5.4 Bubble volume for different gas injection velocities. 51
5.5 Bubble rise velocity for different gas injection velocities. 52

A.1 Transport properties file. 61

A.2 Turbulence properties file. 62
A.3 Gravity file. 62
A.4 ControlDict file. 63
A.5 FvSchemes file. 64
A.6 FvSolution file. 65
A.7 SetFields file. 66
A.8 BlockMeshDict macro file. 69
A.9 Alpha file. 70
A.10Pressure file. 71
A.11Velocity file. 72

B.1 Different views of the parallelepiped volume meshed. 73
B.2 Views of the mesh in the cylindrical volume. 74

LIST OF TABLES

2.1 Characteristic dimensionless numbers. 19

3.1 Characteristic dimensionless numbers of the simulations. 26

4.1 Error percentage compared to the most refined mesh. 37
4.2 Error percentage compared to the smallest time step. 40

LIST OF SYMBOLS

Δx	Cell size
Δt	Time step
α	Fluid phase fraction
$\varnothing_c$	Diameter of a capillary channel
ρ_l	Liquid density
ρ_g	Gas density
μ_l	Liquid dynamic viscosity
μ_g	Gas dynamic viscosity
ν_l	Liquid kinematic viscosity
ν_g	Gas kinematic viscosity
U_{sg}	Superficial gas velocity
V_b	Bubble volume
U_b	Bubble rise velocity
g	Gravitational acceleration
h_v	Height of the vessel
$\varnothing_v$	Diameter of the vessel
τ_v	Viscose stresses
τ_t	Turbulent stresses
F_σ	Surface tension force
σ	Surface tension constant
k	Mean curvature of the free surface
A_c	Capillary cross-section area
t_d	Detachment time
F_b	Buoyancy force
Co	Courant number
Re	Reynolds number
Bo	Bond number
We	Weber number
θ	Contact angle

ACKNOWLEDGEMENTS

First and foremost, I have to thank my advisor Dr. Santiago Arias Calderón, who has assisted me along this project. Without his dedication and involvement in every step done, the final result would have never been the same. Since Santiago Arias offered me the possibility to carry out a research project about CFD numerical analysis in hypergravity conditions, he has provided me all the information and material required to perform the study, in addition to constant follow-up giving me support.

I would also like to show gratitude to Mireia García, the computer technician who has helped me with any software problems and other technical issues regarding the computer that I have used remotely for the simulations.

Last but not the least, I am really thankful to my family who has encouraged me throughout the different stages of the project, specially when I was stuck.

INTRODUCTION

The interaction between fluids in outer space environments is a situation that nowadays humans are more used to face, even though from the first spatial flight, the technology applied in the spaceships and the research carried out by different generations have coexisted with very changed gravity values than the ones on the earth, and this has supposed a real headache for scientists. The gravity conditions that we find in our planet have set up the human mindset, so we expect things to behave in a way which is usual for us. First of all, it is important to describe the concept of gravitation. What is gravity? Which effects come with it? Gravity is a natural force that pulls together all matter (something with mass or energy). This phenomenon piqued the interest of some of the most recognised scientists such as Isaac Newton or Albert Einstein. The first one stated with the law of universal gravitation that every particle attracts every other particle in the universe with a force which is directly proportional to the product of their masses and inversely proportional to the square of the distance between their centres. Even so, nearly three centuries later, Albert Einstein described modern physics gravitation in the general theory of relativity stating that it was a geometric property of space and time. Particularly, he related directly the curvature of space-time with the energy and momentum of whatever matter. Once the most important ideas of the classical and modern scientific periods are presented, it can be pointed the fact that the more matter, the more gravity has a body. Therefore, its gravitational field can reach more distant bodies and the intensity of the interaction with other objects would be larger. Furthermore, when it acts on something, there is always an effect usually from other forces counter acting it. However, the shape of the whole universe is determined by this phenomenon due to the attraction between objects. Satellites orbiting planets, planetary systems around stars or galaxies are some of the configurations making up the universe and all of them are ensured by gravitation.

The earth's gravity is the responsible to keep our feet on the ground and as a counter act, the ground push back on us with a force on opposite direction which we perceive as weight. Because of that, in bodies with different mass as for example the moon where our weight changes, in this case reducing due to the gravitation, is lower as the satellite have less matter than our planet. The gravitational field have an impact not only on things that belong to it but other bodies such as the moon, solar system planets, asteroids, and comets among others. For the same reason, large quantities of matter cause effects on the terrestrial globe. Since the moon is our closest neighbour, and it is a very massive object it exerts a strong gravitational pull on the earth. It is not strong enough for us to feel, or to affect the continents, but it does have a large effect on the world's ocean pulling upwards the water creating the high tides when the separation distance is the lowest and low tides in the other case. Actually, the life on this planet has been set up by the conditions that exist, and all the creations done by humans have been designed to put up with terrestrial gravity. The problem appears when gravity conditions change. This entails a challenge for humans, in the space or in other bodies with much more matter, where microgravity or hyper-gravity can be found.

As gravity force, indeed, is the result of the very nature of matter, affects to all the processes that we can imagine, such as the geologic, biologic, etc... For this reason, sometimes it is desired to carry out experiments without gravity effects in order to understand and study how physic phenomenon and biologic processes behave. The problem is that

meeting zero g condition will imply reaching a point in the universe infinitely remote, and this is not possible. Nevertheless, it is one thing to suppress gravity, which is impossible, and another to suppress its effects, that is, to achieve conditions or reference systems that behave without gravitational effects as if the force of gravity did not exist. Therefore, scientist have chosen the term of microgravity in order to refer precisely to those conditions in which an object is only subjected to very weak gravitational forces.

On the one hand, there is the concept of microgravity, related with the terrestrial gravity value near to zero, and it is expressed as $10^{-6}g$ [2], but as this value is hard to achieve, it can be also considered microgravity from $10^{-2}g$. There are some different ways to achieve microgravity:

- Free fall is one of the most used methods to carry out experiments with microgravity. The absence of a surface that responds opposing to the force of gravity, generates for a short moment of time these values of gravity. The most common ways to generate microgravity are the free fall towers and free fall flights that can produce the desired conditions in the top of the parabolic trajectory for 30 seconds approximately, a fairly high time compared with the case of the tower.

- Orbital capsules or stations that revolve around the Earth, in which the expected values of gravity are accomplished. For example, the microgravity conditions that take place within the ISS (International Space Station) are not due to their distance from the Earth but to their orbital movement around it that reproduce a prolonged free fall.

- Magnetism is also used for this application. The magnetic fields can generate forces that oppose to gravity resulting a total force equal to zero.

Therefore, the rate of progress in microgravity field is very slow and hard due to the little access to infrastructures where can be conducted an experiment under these conditions, in addition to the high costs that would imply, just like it happens to put an experiment on board of the ISS (International Space Station). Despite how much remains to be found out, there are a lot of studies being carried out. Some of them are related with the life in microgravity to understand the effects of these conditions on cells and living organisms. This topic is really important because there are a lot of space missions crewed by humans or other living beings which have to adapt to very different gravity conditions. Health symptoms that astronauts often experience in micro-g are: space motion sickness that is caused by changes in g-forces, which affect spatial orientation in humans, muscular and skeletal disorders as well as loss of muscle or bone decreased mineral density, and cardiovascular problems due to the system is less strained than on Earth. Also, commercial applications experiments are being developed in micro-g such as growing crystals in an attempt to reduce crystal lattice defects for certain microelectronic applications and subsequent X-ray crystallography. Another wide field of study in microgravity is the behaviour of the matter that interact in our technological processes, for example combustion in rocket engines or refrigeration systems with fluids. Even the most natural biological processes including digestion, pumping blood or physiological needs are affected by effects of zero gravity.

On the other hand, we found another particular type of altered gravity, in this case hypergravity. To understand the concept it is essential to know when hyper-gravity conditions

are met. This phenomenon occurs when the gravity value exceeds the one on the Earth's surface. Therefore, as the gravity field is related with the quantity of matter; in the outer space where there are planets, stars or other heavier bodies; we can met hypergravity conditions. Even so, on earth there have been designed machines that can recreate these environments, as well as some experiments designed to reach higher values than g. These are described below:

- Centrifuge machines, that are optimized for spinning a rotor at high speeds and as a consequence generate accelerations with higher values than g. With a full range of gravity levels at their disposal, gravity becomes just another variable for scientists in the laboratory. Nowadays, there are investigations with bacteria carried out in a ultracentrifuge capable of generating around 10^6 g [3].
- Parabolic flights as the ones explained before, where in the top of the trajectory microgravity is achieved, but during the climb and the stabilization phase after the descent, hyper-gravity is reached. The figure 1 shows in detail this experiment.

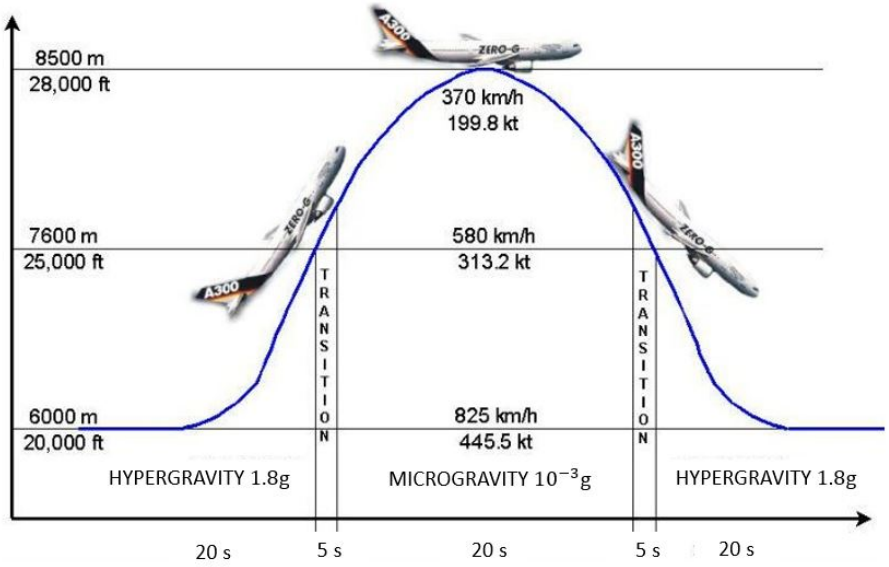

Figure 1: Gravity conditions during parabolic flight.

The applications of these methods that generate hyper-gravity environments have spread from the investigation of human physiology to study the body adjustment under altered gravity, to the testing of materials for space missions, passing through the research of bacteria that can live and breed under gravity values around 400 times g [3]. Most of the experiments carried out with humans have had the aim of preparing astronauts to what they are going to be exposed during the voyages on the spaceships. Furthermore, there are some researches (e.g. Cohen, 2003) that find beneficial effects of being subjected to hyper-gravity. In the 20g centrifuge at NASA Ames, Cohen exposed humans to gravity levels as high as 2g with medical monitoring systems. The conclusions of the experiment were the following:

- Hyper-gravity could be used to train athletes due to exercises would provide more benefit in less time, just like to treat people who suffer from muscle atrophy.

- Centrifuges could be the key to long-term space travels, because microgravity causes the body to deteriorate in a multitude of ways, as explained above, and artificial gravity could prevent all that.

Most of the aerospace research and analysis in high gravity levels have been studying the performance of some materials and testing structures, mostly for spaceships, but also for aircraft. The industrial applications where these conditions are met, basically focus on making spacecraft's components the more resistant as possible to ensure that each structural component will support without damages the different g levels. Some researchers of the European Space Agency (ESA) have been exploring about manufacturing titanium aluminide turbine blades in 20g [4]. But, there are still a lot of issues that appear when changing gravity levels. As you can see, the hyper-gravity conditions research is quite recent just like microgravity. The need of studying these particular situations has been arisen by the progress in space missions accompanied by the remarkable development of science and technology.

Thus far, most of the aerospace research and analysis in high gravity levels have been studying the performance of some materials and testing structures, mostly for spaceships, but also for aircraft. The main objective of these investigations is to ensure that each structural component will support and resist without damages the different g levels.

Therefore, the fact incited researchers to investigate about this fields in order to know and understand the behaviour of things in micro and hyper gravity. As the complexity of the problem is really challenging, the studies done up to now have discovered just a little part of a very unknown and complex topic, so there is still a lot to find out.

Fluids in altered gravity conditions

Considering both gravity conditions, we are going to focus on a specific state of matter, the fluid. This state includes liquids, gases and plasma, but the last one is beyond the scope of this work. A fluid is a substance that continually deforms under an applied shear stress and cannot resist any shear force applied. In addition, a very important and characteristic property is that fluids have the ability to flow, or in other words, they can take on the shape of its container. All the properties mentioned are typically due to their inability to support a shear stress in static equilibrium, contrary to solids that respond to it either with a spring-like restoring force or requiring a certain initial stress before they deform. Then, shear stress in fluids is a function of strain rate. Consequently to this behaviour it appears Pascal's law, which describes that a change in pressure at any point in an enclosed fluid at rest is transmitted undiminished to all points in the fluid. A categorization of fluids depending on the mentioned variables are: newtonian fluids where stress is directly related to the strain rate, or non-newtonian fluids where the relation is not proportional. Moreover, it should be remarked that Navier-Stokes equations describe the behaviour of this state of matter and are based on the conservation of mass, linear and angular momentum, and conservation of energy.

Regarding to fluids, they not only exist in a single-phase, that is, totally liquid or gas. Sometimes, a fluid is made up of a mixture of gas and liquid, and they are called biphasic or two-phase fluids. These ones have very characteristic behaviours due to the coexistence of both phases, each one with different particularities. In this work, we focus on this

particular fluid because it is the most common in human nature and in technological or biological processes. Therefore, the interaction of these phases is an important field of study with the main objective of understanding its behaviour in conditions where their properties are highly altered. So, at this stage, it would be important to wonder what would happen if we change the gravity level at which both liquids or gases are subjected in earth.

First of all, as the environment has changed the behaviour of these fluids will be significantly different than the one that we could expect. In the case of microgravity, hydrostatic pressure in liquids is reduced and its shape is controlled by surface tensions; then smaller free liquid surfaces can be formed in these environment, like liquid bridges and foams. There are some experiments in which gases and liquids are involved, for example combustion. These ones have been performed by NASA's researchers whom have observed a different shape of the flame in zero g conditions compared with the flame which we are accustomed. As a result of gravity, hot air raises and draws fresh cool air behind it, what we call convection, and this is the cause of the flame shooting up and flickering. Nonetheless, in microgravity as there is no buoyancy force, the flame do not acquire a slender shape and as it can be seen in figure 2, it looks like a sphere:

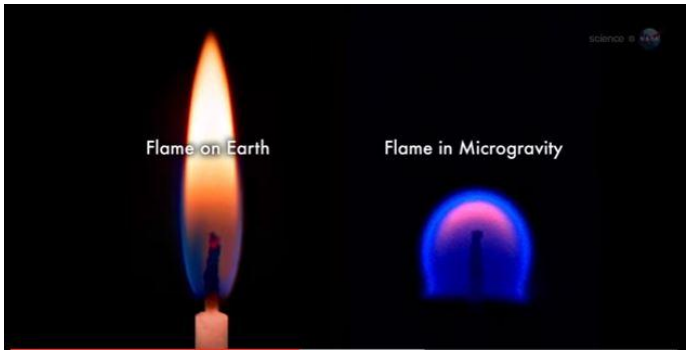

Figure 2: Flame shape on earth versus in microgravity.

Furthermore, microgravity provides the opportunity to achieve a spherical symmetric combustion of a liquid fuel droplet in a still oxidizing atmosphere. This is a classical problem in combustion investigation due to only one spatial dimension enters the description of the burning process thanks to the spherical symmetry. Indeed, it simplifies a lot the mathematics of the problem and for these reason, NASA among others, has used to its advantage zero-g in studies about droplet combustion or flame extinguishment. In short, it is very important to know that either combustion and fires work differently in zero gravity; and both can be extremely hazardous, for example inside a spacecraft. For this reason understanding how fires spread and extinguishes, or how fuels burn in microgravity could improve the efficiency of fuel mixtures used for interplanetary missions by reducing cost and weight, and besides, it could lead to improved safety measures for manned spacecraft.

As mentioned above, changing the gravity level can entail some extraordinary benefits in the behaviour of matter or in the mathematics that involve the experiments. Another field of investigation in which biphasic fluids have prominence is the injection of air in a liquid. Two-phase fluid systems, besides weight reduction, also enhance the performance and efficiency in comparison with mono-phase fluid systems. This fact has been reflected in the rise of capillary gas-liquid flows in different modern applications in space systems. Consequently, it has become a prior necessity the full understanding of the behavior of

gas–liquid interactions in different gravity conditions. There are some remarkable applications of these interfaces for example in space bioreactors, hydraulic or pneumatic contactors, life-support systems for human exploration and development of space, thermal management systems including fuel or electronics cooling, and propulsion systems.

Up until now, different methods have been developed to produce controlled biphasic flows in gravity-reduced conditions. Arias and Montlaur [5] perform a three-dimensional numerical study of the bubble generation process and posterior dispersion into a continuous liquid in a micro T-Junction. This research was a continuation of a previous study done by Arias et al. [6]. This was based on a two-dimensional fluid dynamics numerical study about the formation of bubbles, with a diameter on the order of 10^{-3}m, also in a T-Junction. The parameters studied in these investigations were: bubble size, bubble velocity, volume void fraction, bubble generation frequency and characteristic bubble lengths; with the aim of understanding the behaviour of the bubbles in this environment. As mentioned before, in micro-g environments the effects of gravity are neglected and this, lead to some issues such as the non presence of the buoyancy force that would cause the bubble detachment of the gas injector in a liquid environment. As a result, the bubble increases its volume blocking the injection orifice (figure 3), fact that provokes very negative consequences. For that reason, the T-Junction was thought as a way of solving this problem taking advantage from the liquid flow to force the detachment of the bubble.

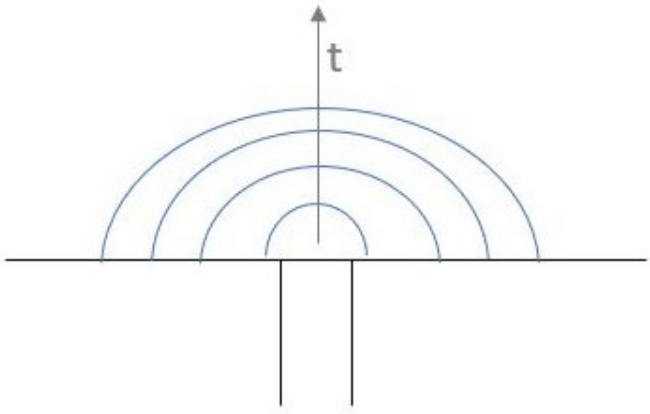

Figure 3: Bubble formation from a capillary in microgravity conditions.

Regarding to two-phase fluids in hypergravity conditions, they behave in a different way too. The problem is that the field of fluids in high gravity environments is very unknown due to there are few investigations and most of them are not about the interaction of the gas with the liquid, but they study other phenomenons in which those fluids are involved. That is the main reason why the interest of this research will focus on the control of bubble dynamics issue in a liquid phase, so systems with bubbly flows, for instance gas-liquid reactors where bubble formation and rise are essential phenomena contributing to its hydrodynamics [7], could be improved and applied in more situations where hypergravity is present. But first of all, it is going to be introduced the subject of rising bubbles.

Rising bubbles

The progress in the mentioned field has been the result of many researchers. In some instances, the aim of the study has been the shape of the rising bubbles in a liquid [8], like for example the water, considering the flow rate of the gas that is being introduced from a nozzle (which is strongly related with the detachment of the bubble) and determined by buoyancy and surface tension forces as well as gravity level.

The bubble paths has supposed another important area of investigation due to it varies depending on the size and the rising velocities of them, but the most important fact is the instability of these paths. It has been proved that before the path becomes unstable, the bubbles follow a vertical path. Once a critical value is reached, the instability appears and then the trajectory becomes a zig-zag or a helical path [1].

Depending on the bubble size, the straight ascension can remain during more or less time and then the path becomes unstable. For smaller bubbles, the duration of the vertical rise is longer, while bigger ones become unstable earlier and therefore, there is a transition to a zig-zag and helical paths [9]. It has been studied that these oscillating trajectories are caused because of the lift force, which is perpendicular to the bubble motion, generated by the wake vortices. The physical causes of path instability can be divided into two. On the one hand, they can be related to the evolution of hydrodynamical forces and torques when a disturbance is applied to the bubble. On the other hand, they can be provoked by the wake instability that occurs in some parameter regimes. Moreover, experiments performed by Zenit and Magnaudet demonstrate that the main parameter to trigger the instability is the bubble shape and not the Reynolds number, because the vorticity generated at the bubble surface mostly depends on the bubble aspect ratio [10]. The properties of the liquid-gas interface, including viscosity and density, have an important role in the results of the experiments being performed, as well as the gravity conditions.

F. Suñol and R. González-Cinca conducted an experimental analysis of the effects of gravity level on the formation and rise dynamics of bubbles. The experiments were performed in the LDC (Large-Diameter Centrifuge) of the European Space Agency to generate a hypergravity environment for millimetre-diameter bubbles. They realised that bubble detachment from a nozzle was determined by buoyancy and surface tension forces. After this separation, the trajectory of the bubble was affected directly by Coriolis force deviating it. Subsequent bubble rise was dominated by inertial forces and followed a zig-zag trajectory with amplitude and frequency dependent on the gravity level. They also connected the gravity with the vorticity, so the increase of this acceleration enhanced the other parameter, which destabilizes the flow and therefore the bubble path [1].

Figure 4: ESA's LDC generating high-gravity levels.

The starting point of this final degree project is the experimental research done by Suñol and González-Cinca [1]. So, the motivation will be the recreation of that experiment, carried out at ESA's facilities, by numerical analysis using an open source CFD (Computational Fluid Dynamics) software, called OpenFOAM, and try to obtain results similar to the ones achieved in the LDC some years ago.

The interest of using CFD programs is to solve and analyse problems where liquids and gases interact inside a volume defined by boundary conditions with no need of using high technology machines in large adapted facilities, which implies very high costs. Nowadays, more and more CFDs are being used for investigations in order to obtain results and analyse them applying numerical simulation and post-processing tools. Therefore, the computers are responsible of performing those computation processes simulating free-stream flows of the fluids and its interactions with surfaces defined previously by boundary conditions.

As the amount of data managed in CFD analysis is really high, the processing capacity is a determinant factor and that is why high-speed supercomputers can achieve better solutions as well as they are often required to solve the largest and most complex problems. The software's scope includes research and engineering problems in many fields of study, such as: weather simulation, industrial system design and analysis, fluid flows, biological engineering, engine and combustion analysis, environmental engineering, and aerodynamics and aerospace analysis. For this particular project, the field of study will be a blend of fluid flow and aerospace analysis, due to the experiment is based in the dynamics of bubbles rising in still distilled-water under hipergravity conditions.

Thus far, the study of two-phase fluids in hypergravity conditions is such an unexplored field, which makes this project really challenging as well as interesting for the progress on this research branch. The main goal of the CFD numerical study will be understanding its behaviour in hypergravity, in order to predict anomalies in systems that work with liquid-gas interfaces and also for improving them in terms of performance or weight efficiency. This may entail important benefits in terms of cost savings and reaching more distant targets.

CHAPTER 1. THEORETICAL FRAMEWORK

This chapter is a compilation of the different theoretical concepts that appear throughout the project and refer to characteristics of some technical aspects of the problem, such as the type of interaction between the fluid and the solid walls determined by the contact angle, fluid properties and work regime characterized by the most relevant dimensionless numbers of the study (Re, Bo and We), and also a condition corresponding to the numerical simulations that is the one responsible for its convergence, the Courant number.

1.1. Contact angle

The contact angle, θ, is a fundamental physical parameter to characterize the hydrophilicity and wettability properties of a solid surface. Moreover, it is defined as the angle at which liquid-vapor interface converges with the mentioned solid surface. The value of the contact angle depends mainly on the relationship between the adhesive forces between the fluid and the solid and the cohesive forces of the fluid interface.

Before the definition of the contact angle in OpenFOAM, it is important to introduce two concepts regarding the materials classification depending on θ. On the one hand the hydrophilic surfaces are the ones that attract water and its contact angle is smaller than 90^o. On the other hand, hydrophobic surfaces seemingly repel masses of water, so the substrate is not moistened, and the corresponding contact angles are greater than 90^o.

The figure 1.1 is a graphic representation of how is defined the contact angle θ according to [11].

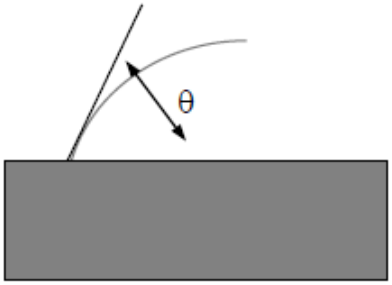

Figure 1.1: Contact angle definition.

From the figure definition it can be checked that for $\theta < 90^o$ the fluid spreads more over the solid surface, so the material behaves in an hydrophilic way, unlike to $\theta > 90^o$ that corresponds to hydrophobic materials in which the fluids spread much less.

Therefore, the contact angle in OpenFOAM has been defined following this criteria and considering that if the material is more hydrophilic, the bubble advance on the solid surface is reduced as the liquid is more spread over the surface. Furthermore, the software recognizes the parameter in question as a boundary condition in the file where are set the fluid phases of the problem.

1.2. Dimensionless numbers

The main interest of this project is the study of a two-phase fluid in higher gravity levels than the one on the Earth. As the experiment is performed inside a millimetric cylindrical vessel, the influence of forces, like surface tension and buoyancy, or the gravitational effects are different to the normal behaviour. That is the reason why there have been used dimensionless parameters straightly related to the fluid properties to understand the influence of the problem initial conditions with the fluid behaviour. Besides, it is important to define how to run a robust simulation in terms of stability and accuracy, which leads to an important concept for numerical analysis such us the one performed in this project.

1.2.1. *Re*, *Bo* and *We*

The Reynolds number (*Re*) is the ratio between inertial and viscous forces of a fluid subjected to internal movement due to different fluid velocities. This dimensionless quantity helps to predict flow patterns according to the type of fluid flow conditions. On the one hand, at low values fluid flow tend to be laminar, which refers to fluid particles following smooth paths in parallel layers with little or no mixing. On the other hand, at high Re the flow is considered turbulent, which implies fluid motion characterized by chaotic changes in pressure and velocity fields. Moreover, it can be said that in laminar flows viscous forces are dominant, while turbulent flows are dominated by inertial forces. According to [12], for $Re < 2300$ it is considered a laminar work regime, while a turbulent flow is not achieved until $Re > 2900$ are reached. The dimensionless number can be defined as: $Re = \frac{\rho U \varnothing_c}{\mu}$, where ρ and μ are the density and dynamic viscosity of the fluid, U is the fluid's velocity and $\varnothing_c$ the diameter of the capillary. But for the current project it will be studied a particular two-phase fluid, so the Reynolds number would be determined as $Re = \frac{\rho_l U_b \varnothing_c}{\mu_l}$, where the subscript l indicates liquid and U_b corresponds to the bubble rise velocity. The *Re* has a large number of applications, ranging from liquid flow in a pipe to the passage of air over an aircraft wing. Although, the most common function of this parameter is to predict the transition from laminar to turbulent flow, one of the most useful application is in the scaling of similar but different-sized flow situations (dynamic similitude), such as a test of an aircraft model in a wind tunnel and the full size version, which implies large money savings.

Another important parameter concerning the characterization of the fluid is the Bond number *Bo*. This dimensionless number represents the balance between gravitational forces and surface tension forces, and can be used to define the shape of drops or bubbles moving in a surrounding fluid. The Bond number is commonly defined as: $\frac{(\rho_l - \rho_g) g L^2}{\sigma}$, where ρ_l and ρ_g are the liquid and gas densities, g represents the gravitational acceleration on the Earth's surface, L is a specific distance and σ the surface tension between both fluids. From the last expression it can be noticed that generally ρ_l is much larger than ρ_g, which leads to the following simplification: $\Delta\rho \approx \rho_l$. Then, as the problem consists in the injection of air, by means of a millimetric capillary, in the bottom of a cylindrical vessel filled of liquid, the final expression to compute this parameter is: $Bo = \frac{\rho_l g \varnothing_c^2}{\sigma}$. A high value of *Bo* signifies that the system is relatively unaffected by surface tension effects, whereas a low value indicates that gravity plays a small role because surface tension forces are dominating. Following the criterion developed by Suo and Griffith in [13], if $Bo < 0.29$ the gravitational forces become negligible in comparison with the capillary effects, so the

bubble generation and detachment process are dominated respectively by surface tension and capillary forces. For this work, it is expected to obtain high values of the Bond number, as the simulation are defined in hypergravity conditions.

The Weber number (*We*) is the last dimensionless parameter used in this project in order to define the fluid properties regarding the different forces acting on or within it. *We* is useful for analysing fluid flows where there is an interface between different types of fluid, primarily in multiphase fluid flows, as it happens in the problem that will be studied. For this specific case it is desired to compute the gas Weber number, which can be defined as: $We = \frac{\rho_g \varnothing_c U_b^2}{\sigma}$. This dimensionless number measures the relative importance of the fluid's inertia compared to its surface tension. So when it is accomplished the following criterion: $We < 2$, capillary forces overcome inertial ones. Thus, the formation process of the bubble is controlled by surface tension forces according to Rezkallah [14].

The values of the mentioned dimensionless numbers can be found in the following sections. The ones regarding the experiment in the LDC are presented in subsection 2.1.2. (Table 2.1), whereas the values corresponding to this project are showed in subsection 3.3.3. (Table 3.1).

1.2.2. Courant number

In terms of the fluid properties and its work regime, *Re*, *Bo* and *We* are the three dimensionless parameters used. Even so, along the study in OpenFOAM there is also another concept, regarding the variation of the time passage of the simulations, that must be introduced in this section.

The Courant number, *Co*, is a required parameter for convergence in numerical analysis when it is pretend to solve partial differential equations. It must be fulfilled $Co \leq 1$ to achieve the stability and correctness required [15]. That dimensionless number can be defined for one cell as: $Co = \frac{\Delta t |U|}{\Delta x}$, where Δt is the time step of the simulation, Δx the cell size in a specific direction and U the velocity of the fluid. From the theoretical expression, it can be seen a straight dependence between Courant, Δt, Δx and the velocity in the direction of Δx. In addition, the *Co* indicates whether the mesh and the time step are accurate enough to capture the physical phenomenon you want to recreate. Focusing on Δt and Δx, these are variables that determine the number of iterations and the mesh refinement of the simulation. As a consequence, there must be a balance between the magnitude order of this variables to keep $Co \leq 1$ throughout the simulation, time, otherwise the simulation's *Co* increases, which leads to either mistaken results or processing errors.

CHAPTER 2. PROBLEM STATEMENT

This project is based in the experiment carried out by F. Suñol and R. González-Cinca about the effects of gravity level on bubble formation and rise in low viscosity levels [1]. Therefore, the interest will be the comparison of those experimental results with the ones obtained in this project using OpenFOAM. But before the discussion of the results, it is important to understand how can be performed the same study by these two completely different ways.

2.1. Background

The aim of this section is to introduce in more detail the work done by Suñol and Cinca about the influence of gravity in two-phase fluids, regarding not only the theoretical part but also the experimental one.

2.1.1. Theoretical framework of the experiment

The purpose of that research was to understand the behaviour of rising bubbles in a liquid phase, while changing gravity levels to hyper gravity conditions. At the time, this study was pioneering and original, just like this CFD study. Actually, this is an issue that affects the performance of some industrial systems that are carried on board or as a structural component of different aircraft and spacecraft. The latter are more affected than aircraft because they experience highest g levels and therefore, they have to be considered as the most critical.

The bubble formation process determines the bubble size depending on the physicochemical properties of the gas-liquid system and the gas injector configuration, whereas the rise velocity governs the characteristic contact time between the phases [1]. Regarding the bubble formation process and shape, they observed some special characteristics in the hypergravity environment generated by the ESA's LDC. For a fixed gas injector diameter, the size of the bubble is established by the balance between surface tension and gravity. Moreover, as the system of their experiment was tested in different gravities, the known deformation that suffer millimetric bubbles was aggravated changing the hydrodynamics and rise trajectories.

As explained in their article, after detachment from the nozzle, bubbles accelerate upward following a vertical path. Depending on the bubble-liquid interface properties, the path can become rapidly unstable due to perturbations applied to the bubble, as for example, wake instability. After detachment, the bubble trajectory is deviated by Coriolis force, which leads to an oscillatory trajectory, during the rise, at all gravity levels considered for that experiment. Suñol and Cinca detected a variation on the frequency and amplitude of the paths related with gravity level changes. Specifically, as gravity increases, trajectories have larger frequencies (more oscillations) and lower amplitudes. They captured this phenomenon with a special camera once a steady gas flow rate was reached. The resulting images can be seen in the figure 2.1:

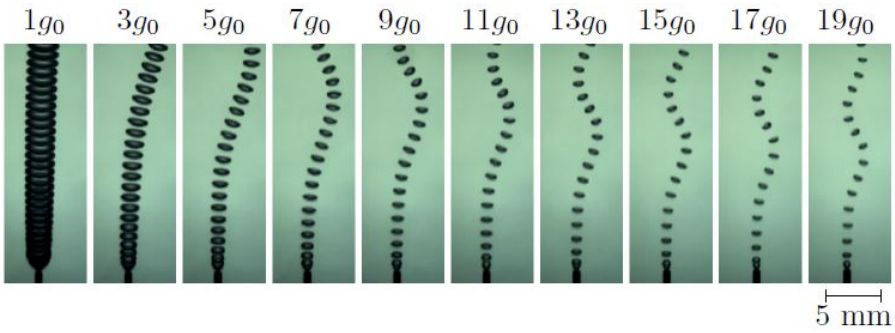

Figure 2.1: Bubble detachment and rise for a steady flow.

Although Coriolis provokes a deviation of the bubble rise path, it doesn't play any important role in the zig-zag. Other significant feature found by them was that despite bubbles of the size considered in their hipergravity tests followed a rectilinear trajectory in normal gravity, it was seen that at larger g values, the vorticity produced at the bubble surface increases enough to produce a wake that destabilizes the flow and induces the mentioned zig-zag trajectory.

Experiments performed by Wu and Gharib [16], proved that a bubble formed by inflating it at an injector will normally show an ellipsoidal shape because of the pinch-off event perturbation, and rise in a helical or spiral path. However, when the bubble is delicately released from the injector, it can maintain a spherical shape, but the rise velocity will be lower in comparison with the previous bubble. Furthermore, the rise of spherical bubbles follows a rectilinear trajectory or a smooth zig-zag motion in contrast to the ellipsoidal-shape bubbles that perform either an helicoidal ascent or a zig-zag path.

2.1.2. Experiment set-up

The set-up of the experiment, in which this project is based, was designed to be performed in the ESA large-diameter centrifuge, located in Noordwijk (Netherlands). The tests were carried out in that system because it allowed to achieve hypergravity levels from 1g to 20g using the centrifugal force as a source of artificial gravity, thus it provided the required hypergravity environment. More specifically, the experiment was introduced in a gondola that is placed in the end of the LDC's arm, so that can spin at 4 meters from the rotation axis. In the figure 2.2, it can be seen the inside of the gondola:

Figure 2.2: Inside of the gondola where the experiment was placed.

The gondola shown, can also rotate itself from the axis where it is suspended. This leads to another variable that comes into play, the inclination angle of the gondola. The angle is measured with respect to the gravity vector, so the gondola's floor keeps perpendicular to the gravity generated artificially due to the centrifugal force. However, the effects or accelerations associated with this inclination are not taken into account in this CFD project.

In order to see the behaviour of the rising bubbles inside the gondola, they used a camera at 2000 fps to record the bubble column generated by the syringe without missing any details. As it will be explained later, this execution of the experiment is the one aimed to simulate with OpenFOAM by characterising a volume and the fluids of the interface.

Regarding the experimental set-up in the investigation of Suñol and González-Cinca, the air was injected into a tank filled of distilled-water by means of a syringe pump with a stainless steel-nozzle of 0.15 mm diameter. The properties of the fluids used are: $\rho_l = 10^3 kg/m^3$, $\mu_l = 10^{-3} Pa \cdot s$,$\nu_l = 10^{-6} m^2/s$, $\rho_g = 1 kg/m^3$, $\mu_g = 1.8 \cdot 10^{-5} Pa \cdot s$, $\nu_g = 1.48 \cdot 10^{-5} m^2/s$ and a surface tension between both fluid phases of $\sigma = 0.0728 N/m$. Therefore, considering these values there can be computed the corresponding dimensionless numbers *Re*, *Bo* and *We* by means of the theoretical expressions defined in 1.2.1.:

Table 2.1: Characteristic dimensionless numbers.

$U_b(m/s)$	*Re*	*Bo*(1g - 20g)	*We*
0.275	41.25	$3.03 \cdot 10^{-3}$ - 0.061	$1.56 \cdot 10^{-4}$
0.50	75	$3.03 \cdot 10^{-3}$ - 0.061	$5.15 \cdot 10^{-4}$

Even though in [1] doesn't appear the gas injection velocity applied in the experiment, it is said that they reached a low steady rate flow to gently generate bubbles. However, as the parameter required to compute textitRe and textitWe is the rise velocity of the bubble, it has been taken two different values from the results obtained in their experiment, $U_b = 0.275 m/s$ corresponds to the lowest gravity conditions (1g) and $U_b = 0.5 m/s$ to the highest gravity level (20g). From the table 2.1, it can be concluded that the study performed in the LDC was a problem with a laminar flow due to the small Reynolds number of the fluid. The Bond number obtained proves that the detachment is determined by buoyancy and surface tension forces regardless of the gravity level according to the criteria fixed in subsection 1.2.1., since $Bo < 0.29$. Finally, the gas Weber number computed with the fluid properties shows that capillary forces overcome inertial forces, besides the bubble formation is determined by surface tension, also following the inequality in 1.2.1.. Both fluid properties and work regime of the previous investigation will be compared with the ones corresponding with this project in the next chapter.

CHAPTER 3. METHODOLOGY OF THE EXPERIMENT IN OPENFOAM

OpenFOAM is the program that performs the simulations of the experiment done in the LDC. However, this could not be possible without the input files that are created for the case before running the simulation. Some of these are the ones that have the fluid properties and boundary conditions, among other inputs that will be explained below. Thus, it is possible to recreate the behaviour of the biphasic fluid inside a cylindrical volume that pretends to be the vessel.

3.1. The software

OpenFOAM is an open source CFD program with source code based in C++ libraries. As a free license software, it provides a set of tutorials to help the new user become familiar with the program, and at the same time to show the different options that can be used, accordingly to the matter at hand.

For this research, the software has been compiled on Ubuntu, but can run as well with other operating systems. OpenFOAM is a framework for developing application executables that use packaged functionality contained within the mentioned libraries. On the other hand, this software does not have a visual interface, the fact that makes more complicated its use. So, in order to visualize the geometry generated or its mesh, it is used Paraview as complementary program.

The different pre-built applications that offers OpenFOAM can be differentiated in utilities and meshing tools, that are designed for tasks that required data manipulation in the pre-processing; and solvers that are designed to solve a specific problem considering its physico-chemical properties. For the case to study, were air and distilled water interact with the purpose of generating rising bubbles, it has been considered the problem as isothermal, incompressible and laminar; to execute a numerical simulation the most similar as possible to the experiment carried out before. So with these inputs, it is possible to choose the proper solver for running the simulations.

In addition to the applications for pre-processing and solving the problem, there is an important stage after it is done all that, the post-processing of the simulation's data. OpenFOAM is supplied of post-processing environments too, that ensure consistent data handling. The program responsible of that is also ParaView, that allows the visualization of what is happening as if the experiment was not a virtual. The overall structure of the program can be seen in the figure 3.1 below:

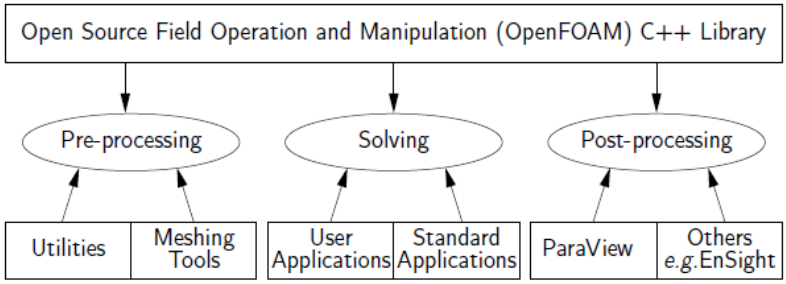

Figure 3.1: OpenFOAM's structure diagram.

As it can be seen, despite the complexity that entails an investigation of this magnitude, CDF software can simulate the exact fluid dynamic conditions as long as the inputs are properly defined. Besides, this signify that an experiment as expensive as the one performed in ESA's facilities could be simulated in a computer, thus the cost of the study would be highly reduced.

3.2. The case structure

The structure corresponding to the case have three main directories: system, constant and 0. The main role of the first directory is for setting parameters associated with the solution procedure itself; the constant directory contains a full description of the case mesh and its properties; and the 0 is the first time directory where can be found individual data files for particular fields. Figure 3.2 shows the general structure state of a case.

The system contains at least three files:

- ***controlDict***: where are set the control parameters of the simulation, *e.g.* start/end time, time step and data output parameters.
- ***fvSchemes***: where discretisation schemes used for the solution can be selected at run-time, depending on the type of problem trying to solve.
- ***fvSolution***: where the equation solvers, field tolerances and more algorithm controls are set for running the simulation.

Constant directory includes the detailed mesh description distributed in different files regarding its points, cells and faces. Furthermore, this folder contains the files where gravity level, fluid properties and type of flow (laminar or turbulent) are defined, so the simulation can make the fluids behave as it is desired.

Lastly, the 0 directory gathers either, boundary conditions and initial values specified by the user in order to define the problem. In the concerning case, not only velocity and pressure files will be found, but the alpha-water also. The latter variable appears in problems were different fluid phases coexist. Principally, the alpha coefficient represents the fluid phase fraction (liquid or gas) inside the experiment volume. Additionally, it is remarkable that, once the simulation is running, more time directories will be created, accordingly with the simulation's *writeTime* defined in *controlDict*, and these files will collect the results computed by OpenFOAM.

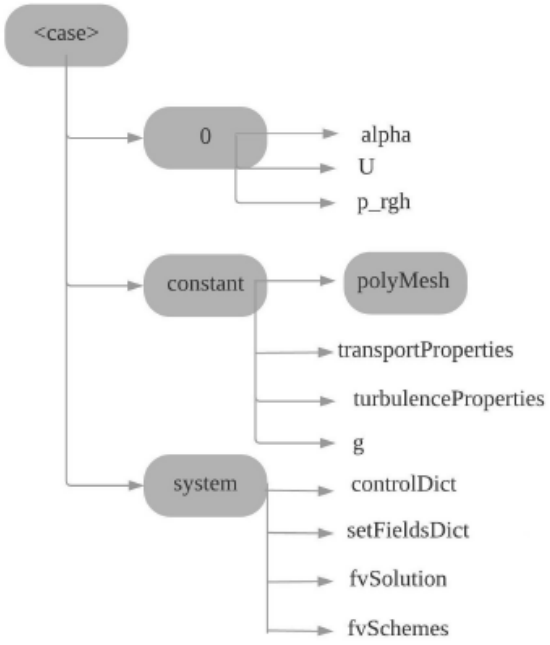

Figure 3.2: Scheme of a general OpenFOAM's folder case structure.

3.3. Pre-Processing

This section provides a specification of the way OpenFOAM handles the preparation of the simulation by means of different utilities that comprise the pre-processing part.

3.3.1. Geometry of the OpenFOAM's volume

The dimensions of the geometry where the experiment has been carried out are based on the one used by Suñol and González-Cinca. They performed the experiment in a vessel (millimetre-scale) filled of distilled-water. The software used for the design of the control volume has been OpenFOAM too. Although in a first instance GMSH was the program chosen for the design, after some tested volumes it was decided to work with the same software that would do the simulations, because in the tests performed appeared several problems when exporting the volume (in the following section will be explained in detail).

The model geometry had a perforation in the center of the base, where a syringe entered to inject air from the bottom. The OpenFOAM's geometry is exactly the same, but with a little modification. Instead of entering a millimetric nozzle, the gas would be injected directly from the perforation at the base of the vessel. Nonetheless, in this project would be attempted to simulate the syringe's surface by adjusting the contact angle value, as this parameter affects directly the interaction between the bubble and the solid surface. In the figure 3.3, it can be observed the difference between both cases.

Figure 3.3: Schematic representation of the bubble stream formation in Suñol and González-Cinca's experiment (left) versus in the virtual experiment (right).

The cylindrical volume could be described considering three main parts: the top of the cylinder, the sides and the base. The top consists in a free surface, so the distilled water would be in contact with the external atmosphere air. The sides of the simulated volume have been considered as walls, in order to reproduce the conditions inside a vessel. Finally, the most critical part of the geometry, the lower base of the cylinder where the central part is a gas injector orifice and its surroundings are walls. In the following figure there are different views of the geometry:

Figure 3.4: OpenFOAM's geometry frontal and vertical views.

In the figure 3.4 it can be seen what fluid phase there is in each part of the vessel, in other words, the figure shows the initial boundary conditions of the fluid problem. The gas is represented in blue as it can be seen in the center of the base (corresponding to the gas injector) and in the top of the cylinder, where the free surface is in contact with the atmosphere (the white colour represents the inter-phase between liquid and gas). On the other hand, the liquid phase is represented in red as it can be observed inside the walls of the volume.

3.3.2. The mesh

The mesh concept is related to a network set up by cells and points. Its most notable feature is the ability to adapt, so that it can almost have any size and shape. The mesh is used to solve partial differential equations where each cell represents an individual solution of the equation which, when combined for the whole network, results in a solution for the entire mesh. The way to obtain the problem solution can't be solving the entire problem domain at once due to the complexity that carries intrinsically the volume. Obviously, the creation of the grid is one of the most important stages in a numerical study simulation since the final result depends on how good and refined it is. This is the reason why an important part of the project has been spent in the mesh generation.

Some of the things that were taken into account when designing the volume's mesh were the need of a more refined grid from the gas injection area to the vessel's top, and a continuous degradation of the mesh density as the distance from the centre increases. That variation in the mesh was conceived to achieve a better precision in the computations that would happen in critical areas, for example where the bubble formation and detachment processes would take place, as well as the area for which the bubbles would rise. Other mesh considerations were the complex geometries like corners and angles that can make extremely difficult for solvers to obtain a solution. On the other hand, small cells are comparably easy to solve and therefore the applied strategy.

The principal drawback of using OpenFOAM was the lack of a visual interface that complicated the meshing task. Moreover, the grid creation process was not parametrized, fact that slowed down the work. But lastly, through the use of a macro (m4 file) created by the mechanical engineer Ehsan Madadi [17], it was possible the generation of a cylindrical volume meshed by applying trigonometric functions. In contrast, the main advantages of this macro are: the automation of the blockMesh file creation, the one in charge of the mesh generation; and the parametrization of the problem that defines the volume and the mesh, which speeds up the processes of creation and modification of the grid. The final mesh achieved with this macro can be seen in the figure 3.5.

In Appendix B, a wide explanation of the mesh generation can be found.

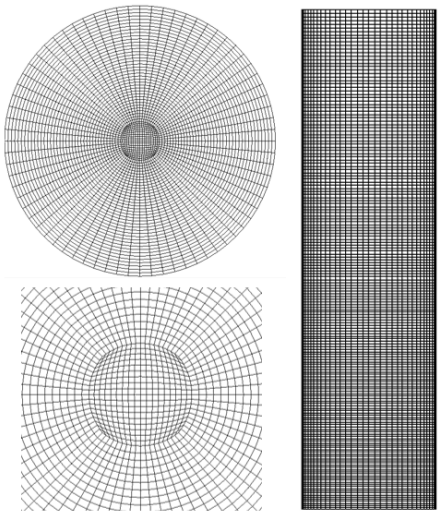

Figure 3.5: Views of the mesh generated in OpenFOAM by means of the m4 file.

As notable aspects of this design it is necessary to summon, on the one hand, the degraded grid from the center of the vessel to the limits of the geometry, and on the other hand, the shape of the gas injector that instead of being a perfect circle is a kind of hybrid between a circle and a square, although it looks more like a circle. That peculiarity has been applied to the mesh in order to avoid computation problems during the simulation due to critical geometries such as cells with very small angles.

3.3.3. Fluid properties and dimensionless numbers

The fluid used in the experimental research carried out in the ESA's LDC, as mentioned previously, was a two-phase fluid based in distilled-water and air. Therefore, in the current problem it has been considered the same fluid composition. The particularity of simulating the previous experiment with CFD software is that the fluids that take action in the vessel are no longer real. Then, each fluid phase must be defined with its properties as well as the work regime, so it should be achieved the same behaviour of the real fluid inside the vessel. Furthermore, it is required to define the boundary conditions of the different parts that set up the problem's volume. This would make the fluid interact in the desired way with the solid walls of the cylindrical volume.

Unlike in [1], the internal diameter of the simulated capillary gas injector is: $\varnothing = 1mm$. This value was not selected randomly since different factors were taken into consideration. First of all, it was intended to simulate a capillary of the same dimensions than the one used in the experiment where this project is based, but the fact that the diameter was so small had impact in the parameter Δx, which at the same time unbalanced the *Co* number making the simulation to fail. Then it was decided to fix a similar value which avoid the mentioned error, so after some test it was chosen 1 mm because it accomplished that requirement and at the same time, being unitary would make easier to work with the parameter.

As mentioned above, both phases of the fluid have been considered incompressible and isothermal. The physical properties corresponding to the distilled-water and the air used for the simulations are exactly the same than the values presented in subsection 2.1.2., taken from the research [1]. With them, it has been possible to calculate again the dimensionless numbers *Re*, *Bo* and *We*. The results can be seen in the table 3.1:

Table 3.1: Characteristic dimensionless numbers of the simulations.

$U_b(m/s)$	*Re*	*Bo* (1g - 10g)	*We*
0.21	210	0.135 - 1.35	$6.06 \cdot 10^{-4}$
0.44	440	0.135 - 1.35	$2.66 \cdot 10^{-3}$

Just like in subsection 2.1.2., there have been used the formulae in 1.2.1. to compute the characteristic dimensionless numbers. The bubble rise velocities for which has been computed the three dimensionless numbers are the minimum and maximum values measured in this project, so it can be seen within what limits will be the range of values of the dimensionless numbers. The table 3.1 shows that for the maximum velocity, *Re* and *We* are bigger than for a rise velocity of $0.21m/s$, while the Bond number remains the same due to its non dependence with the U_b. Despite these observable differences, the values of each parameter belong to the same classification. Regarding the Reynolds number, both are far below from the limit value of 2300 according to [12], for which the flow starts

having some turbulences, so our problem can be considered laminar without any doubts. The Bond numbers obtained prove that as it is increased the gravity level, gravity plays a more relevant role. For instance, at 1g $Bo < 0.29$ and then the surface tension dominates in the bubble generation process, as explained in subsection 1.2.1., but for 10g gravitational effects prevail over surface tension effects. Lastly, the gas Weber number proves that capillary forces overcome inertial forces, so the bubble formation and detachment is dominated mostly by surface tension over liquid drag forces, as established in [14].

To conclude this section, it can be said that the dimensionless numbers obtained for the numerical study are similar to the ones computed for the experiment in ESA's LDC, because both investigation are performed in the same fluid working regimes. Nevertheless, some differences have been found in *Re*, *Bo* and *We* owing mostly to the internal capillary diameter of the gas injector. This fact is not a problem due to the study presented in this work is merely an approximation. What really matters is that the dimensionless numbers have the same range and order of magnitude in both studies to obtain similar behaviours of the fluids.

3.3.4. Initial and boundary conditions

The initial conditions of the problem are defined in folder 0, as well as in setFieldsDict file from system directory and g file belonging to the folder constant. In 0 there is a file for each field to measure along the simulation. For the case of study in this project, the different magnitudes of interest are: alpha coefficient, velocity and pressure. Even so, gravity would be introduced also as a initial condition of the problem.

The first parameter can be found in AlphaWaterDict, it defines the alpha coefficient, regarding the fluid phase fraction, for each part of the volume. OpenFOAM has been configured to define this parameter as 1 when is full of water and 0 for air. Consequently, the air inlet and the free surface of the vessel's upper part were set to 0, while the solid walls of the volume were set with alpha equal to 1. To completely define the alpha fraction over the volume, in setFields is defined that the vessel would be filled of water up to a certain point and from there would be air. As for the velocity, in the gas inlet it is imposed the uniform condition and also normal to the bottom surface (vertical direction) with its corresponding value. For the other parts of the geometry the fluid is still so the velocity equals zero. Finally, the gravity level is set in g, even though its value would be changed for each specific simulation depending on the conditions desired, ranging from 1g to 10g.

Furthermore, the boundary conditions are set in directory 0, as mentioned in the case structure at the beginning of this chapter. The gas inlet is defined as a fixed flow in order to inject air to the simulated volume with constant velocity, whereas the outlet has just zero gradient boundary condition. For the walls of the vessel have been assumed the non-slip condition, which implies that the fluid near the solid boundary behaves like it is stuck to the surface. In quantitative terms, that means zero velocity of the fluid relative to the solid boundary.

About the pressure field conditions, either the inlet or the solid walls are defined with fixed flux pressure condition. This boundary condition is used for pressure in situations where zero gradient is generally used, but where forces such as gravity and surface tension are present in the solution equations. In contrast, for the free surface (named as outlet) it is assumed the OpenFOAM's condition of total pressure, where it is determined international

standard atmosphere pressure value of 101325 Pa.

3.4. Processing

The aim of this section is to explain how OpenFOAM can handle simulations of a multiphase fluid flow. Therefore, it is going to get a little bit into the details with the type of solver required in such a case and the equations that must be solved during the numerical analysis. First of all, it must be well known the type of problem that is going to be solved. So, once the work conditions are defined the next step is try to find the solver that fits better with our case.

3.4.1. InterFoam

The conditions of this case, as mentioned in previous chapters, are based in the ones defined in [1]. In order to start the search of the most appropriate solver, it was taken into account the most general property of the experiment, the biphasic fluid. Then, considering this restriction the group was reduced to the multiphase solvers. Within these it was found interFoam, specific for 2 incompressible, isothermal immiscible fluids using a volume of fluid (VOF) phase-fraction based. Some of the most distinguished features of InterFoam are: the ability to capture the interfaces between both phases, as well as including contact angle and surface tension effects for each fluid phase, with optional mesh topology changes.

InterFoam solves the Navier Stokes equations: momentum equation and continuity equation, for both fluid phases. That means that the material properties are the same in the region filled by one of the two fluids except at the interphase [18]. Besides, the fluid's physical properties are computed as weighted averages based on the VOF fraction of both phases in one cell.

The continuity equation 3.1 and momentum equation 3.2 are right below:

$$\frac{\partial u_j}{\partial x_j} = 0 \tag{3.1}$$

$$\frac{\partial(\rho u_i)}{\partial t} + \frac{\partial}{\partial x_j}(\rho u_j u_i) = -\frac{\partial p}{\partial x_i} + \frac{\partial}{\partial x_j}(\tau_{v_{ij}} + \tau_{t_{ij}}) + \rho g_i + f_{\sigma i} \tag{3.2}$$

The density and viscosity are defined by the following expressions:

$$\rho = \alpha\rho_l + (1-\alpha)\rho_g, \tag{3.3}$$

$$\mu = \alpha\mu_l + (1-\alpha)\mu_g, \tag{3.4}$$

where the subscripts l and g correspond, respectively to liquid and gas phases. As mentioned before, $\alpha_l = 1$ and $\alpha_g = 0$, but for the fluid interface, alpha coefficient can be between 0 and 1.

The surface tension $f_{\sigma i}$ is computed as:

$$f_{\sigma i} = \sigma k \frac{\partial \alpha}{\partial x_i}, \tag{3.5}$$

where k is the mean curvature of the free surface, determined by the expression:

$$k = -\frac{\partial}{\partial x_i}\left(\frac{\partial \alpha / \partial x_i}{|\partial \alpha / \partial x_i|})\right), \tag{3.6}$$

The equation 3.7 refers to α coefficient. As it is known, its values in a cell can oscillate between 0 a 1, depending on the volume fraction's value of each fluid in that cell. Then, in order to know where the interphase between the two fluids is, an additional equation for alpha has to be solved:

$$\frac{\partial \alpha}{\partial t} + \frac{\partial (\alpha u_j)}{\partial x_j} = 0 \tag{3.7}$$

This expression can be understood as the conservation of the mixture components along the path of a fluid parcel [18].

With this set of equations are well defined the calculations carried by interFoam during a simulation. So, it can be checked that the solver provided by OpenFOAM fits perfectly with the particular case of study in this project.

3.5. Post-Processing

Post-processing can be performed once the simulation has finished. Therefore, this process is the last part of the project and is based in the analysis of the data obtained. Considering the complexity of the mesh along the geometry and all the calculations that must be performed in each iteration, it can be imagined the huge amount of results taken from each simulation done. For example, a standard simulation can store approximately 100 million data, that in terms of occupied memory would be 5 GB. Since the data management is a really hard task, at least with the resources available in this project, it has been used a post-processing software called ParaView.

ParaView is an open-soure data analysis and visualization program, which lets the user analyse the data by means of its visual interface. So, after OpenFOAM executes the simulation, the data obtained can be quickly build to study with either qualitative or quantitative applications in ParaView's environment. The software gives different options of data exploration such as interactively in 3D or programming using its batch processing capabilities [19]. The software ParaView was developed in order to analyse hugely large datasets by means of distributed memory computing resources. For this reason it can be run on supercomputers, when datasets have petascale size, as much as on regular laptops, for smaller amounts of data. It must be remarked that thanks to this tool, the high performance computation has been incredibly improved. One of the most common applications is for computational fluid dynamics simulations, such as the ones carried out in this project.

In order to perform the volume and velocity measurements, the α coefficient have a key role since it allows to calculate the mentioned parameters for the following chapters. Consequently, OpenFOAM stores the value of alpha (among other parameters) for each cell of the volume, while the simulation is running. The data write time can be defined in system directory, so that the shorter write time, the more data it will store. Then, to check the value of the fluid phase fraction and at the same time, verify the correct generation and rise of the bubbles inside the vessel, it was done a vertical cut to obtain a clear view of the cylinder's central part, where it is injected the air. Alternatively, to compute its value in a particular heigh of the tube, it can be done a perpendicular slice with ParaView and afterwards generate a graph like the one below:

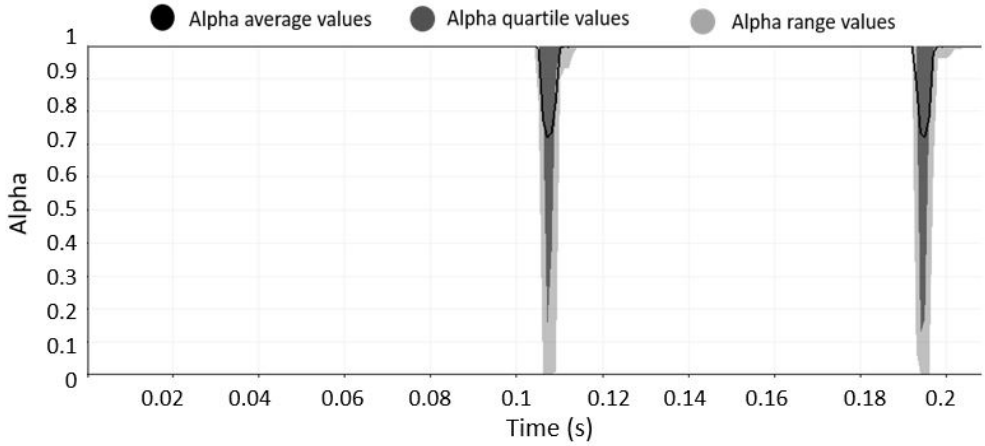

Figure 3.6: Phase fraction as a function of time for $U_{sg} = 0.06 m/s$.

In figure 3.6 can be observed that for a specific area normal to the cylinder's vertical axis, the prevailing fluid phase is liquid, as the value starts and finishes in 1. Nevertheless, there can be seen some oscillations corresponding with the bubble crossing the perpendicular surface along its rise, so each time alpha decreases means that a new bubble has crossed. Figure 3.6 shows different computations of alpha: the black line represents the average values of this parameter, the dark grey area represents the range of values computed in each quartile, and the light grey is for all the range of values calculated for α. Of these three, the only measure of interest that has been used along the project is the average of alpha. This technique has been used for measuring the bubble's rise velocity as it will be explained in the section below.

3.5.1. Bubble volume

The volume of the bubble is measured by means of ParaView's viewer panel. The measurement process consists in sectioning the cylindrical volume by its half in a vertical plane, to be able to observe the development of the bubble inside. So, at the exact moment of the bubble's detachment it is captured the time passed. Therefore, the volume is computed using the following definition:

$$V_b = U_{sg} \cdot A_c \cdot t_d \tag{3.8}$$

where A_c can be easily computed: $A_c = \pi \cdot (\varnothing_c/2)^2$.

3.5.2. Bubble rise velocity

The bubble rise velocity is computed the same way as for the fluid phase fraction, but instead of making one cut perpendicular to the tube where alpha is measured along the time, a second slice is done. Thus, there are two different datasets belonging to different heights over the vertical axis, through which can be computed the time spent by a bubble to cross each section. The velocity of the bubble is defined as:

$$U_b = \frac{\Delta z}{\Delta t} = \frac{z_2 - z_1}{t_2 - t_1} \tag{3.9}$$

It is important to place the lowest section high enough for two main reasons: let the bubble surface stop the heavy oscillations after the detachment and give some time for the bubble's rise velocity to stabilize. Just like the upper surface, that must be located before the point where starts the bubble's lateral oscillation (zig-zag trajectory) since it is pretended to measure the velocity in linear path.

CHAPTER 4. VALIDATIONS

This chapter is one of the most important parts of the project, since the correctness of the subsequent simulations will be determined. Validations are the previous step to the final simulations, from which the data will be extracted and analysed, to compare them with the results corresponding to [1]. This means that depending on how well are defined the set-up parameters, the results obtained would be better or worse. Not only that, but efficiency and accuracy of the simulation might differ significantly.

In order to achieve the best results, as well as the desired behaviour of the fluid, several tests have been carried out. In the following sections it will be explained the contact angle, mesh convergence, time step convergence, bubble formation and influence of the transitory tests, as well as an analysis of the influence of each parameter concerning the simulations outcome.

4.1. Contact angle tests

For the case of study, there is a gas injector from where the bubble is generated, surrounded by a liquid phase, and at the same time contained in a solid vessel. Although in the experiment performed in the ESA's LDC, the conditions where the same, the injection of the gas was performed by a syringe protruding from the base of the container, as showed in preliminary geometry section 3.3.1.. Consequently, during the gas injection the bubbles suffered not only an adhesion with the solid part between the capillary diameter and the syringe diameter, but with the exterior walls of the overhanging nozzle.

However, as it is unknown the contact angle of the experiment in [1] and the material of the solid surface belonging to the tube used, there have been checked different values of the contact angle in order to obtain the one with the most similar behaviour, considering the particular formation process of the bubble owed to the geometry.

Therefore, the simulations generate bubbles from a nozzle, so the contact angle value must be set smaller than 90^o, as explained in 1.1.. At the same time it is defined that the solid walls' material is hydrophilic, to achieve a vertical development of the bubble and prevent any important adhesion with the solid surface that could perturb its behaviour.

In fact, the main objective of the contact angle validation is the determination of the proper angle value that leads to the bubble flow obtained in the experiment performed previously. Thus, different simulations were carried out testing θ from 0^o, value corresponding to a fully hydrophilic material, to 100^o, that is a critical value since above 90^o the materials are becoming hydrophobic. The results obtained are shown in the figure 4.1 below:

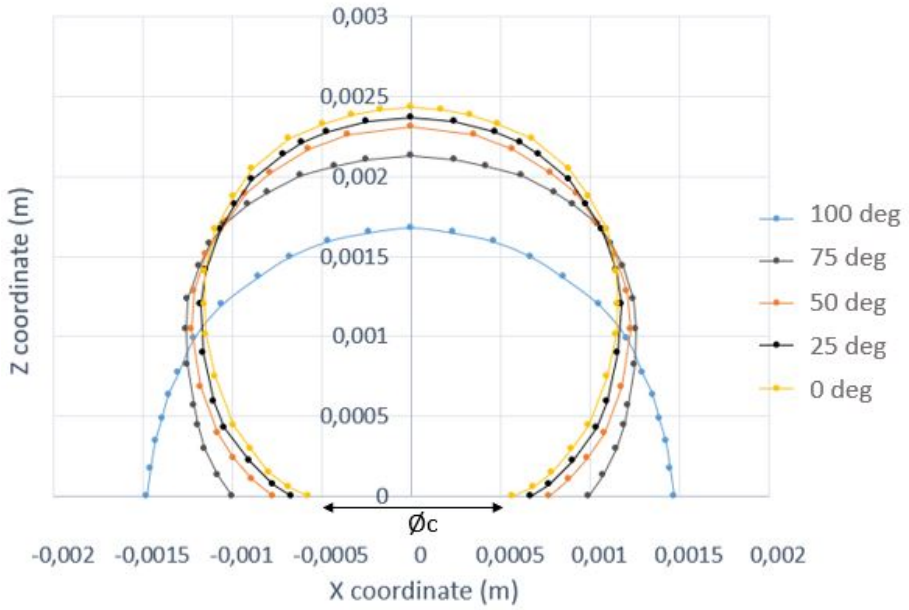

Figure 4.1: Influence of the contact angle in bubble formation at t=0.05s.

This figure contains the contour of a bubble generated from a capillary of $\varnothing_c = 1mm$, for specific values of θ , all of them captured for the same time elapsed. It can be seen that the adhesion of the bubble to the solid surface is greater as it is increased the angle. This can be checked observing the cases of $\theta = 100^o$ and $\theta_{OF} = 0^o$, where it can be appreciated that the first one spreads over the surface, while the base of the other bubble remains in the gas injection area. For the intermediate cases, as the contact angle increases the bubbles are more adhered to the vessel. That result was expected thus the material's hydrophilicity increases for lower values of θ. Moreover, for smaller contact angles, the bubbles are more developed regarding the formation process, which indicates that they are closer to the detachment. Both adhesion and the moment of formation of the bubble depend on the volume and size of the bubble. The figure 4.1 shows the important increase of the bubble's volume for higher contact angles. That is why the most hydrophobic cases (0^o or 25^o) generate bubbles of smaller size (considering that they are in a more advance formation stage). Additionally, the material's hydrophilicity can be related with the time required for the detachment, since the adhesion of the bubble to the vessel's base makes slower the formation process.

Thus, it can be said that the contact angle is straightly related with some bubble properties such as the volume, shape, detachment time and its adhesion with the surface (hidrophilicity of the material). Furthermore, some of the properties mentioned before have influence on other bubble characteristics that appear after de detachment, as for example, the rise velocity or the ascension path. So, it is very important to define properly the contact angle in OpenFOAM because the results obtained in the simulations will strongly depend on it.

Finally, in order to perform the ultimate simulations, it was needed to define a value for the contact angle. So, accordingly with the description at the beginning of this section about the behaviour of the bubbles during the formation process in [1], and after many test simulations for different angles, $\theta = 25^o$ was the definitive value chosen for the following numerical studies of the project. This value was the one selected because it gave better results in terms of similarity to the reference study, since it allowed to achieve a little bit of

adhesion with the vessel's base as well as the material behaved in an hydrophilic way.

4.2. Mesh convergence

Not only is required the validation of the contact angle for the following simulations, but also must be validated the convergence of the mesh. This is a fundamental part considering that the correctness and accuracy of the results will be strongly related with the number of cells of the grid. In order to ensure the best mesh, in terms of precision and efficiency, multiple simulations were performed varying the total number of cells in each of the three axis, and following the criteria established in subsection 3.3.2..

The way to proceed in this study has consisted in multiple simulations classified in five different groups. Each one defined by its number of cells, but at the same time all of them sharing the same physical properties and boundary conditions. For all the simulations, the parameters of velocity and volume have been computed, also for different gravity values. Therefore, in these section it is proved how the results change due to the density of the mesh, and at the same time it is analysed the influence of the gravity regarding the error evolution.

At the beginning, it was intended to test three meshes: a coarse mesh of approximately 145k cells, an intermediate mesh of about 280k cells and a refined one formed by near 535k cells. That number of cells was chosen considering the grids simulated in [5]. As it can be seen in the table 4.1 , the error variation between those cases is very similar. So, in order to prove more evidently the evolution of the results with the decrease of the number of cells, two more coarse meshes were generated: a mesh of 10k cells and another of 5k cells. The refined mesh has been taken as a reference to compare the results since it should produce the best ones.

Moreover, it must be remarked that these simulations were run with the following setup parameters: $U_{sg} = 0.06m/s$, $\varnothing_c$ =0.001 m , h_v =0.022 m and $\varnothing_v$ =0.0035 m, where U_{sg} is the gas injection velocity, $\varnothing_c$ and $\varnothing_v$ are respectively the diameter of the capillary and the vessel, and lastly h_v that corresopnds to the vessel's height. These values and the mesh ones were checked previously with the ones in [1, 5] to assure a correct magnitude order comparing it with both a similar CFD study and the background research of this project.

The figure 4.2 expects to show the difference in the bubble volume computed depending on the mesh's cells density. The main objective of this figure is to prove that as the mesh refinement increases, the result converges, which ensures the correctness of the value.

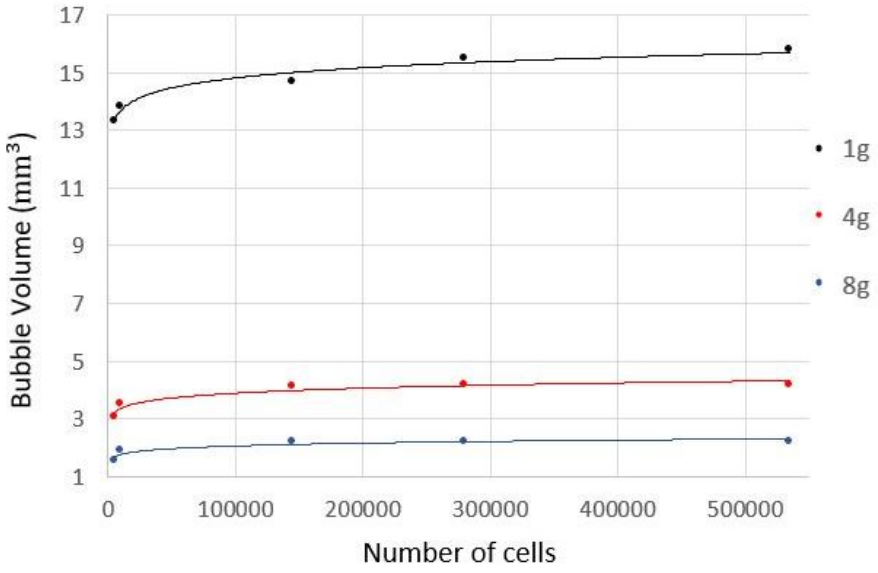

Figure 4.2: Bubble volume as a function of the number of cells for different gravity levels at $U_{sg} = 0.06m/s$.

From the figure above, it can be seen that despite the volume varies for each value of gravity, all the graphs follow the same pattern: firstly, the rate of change in the data increases quickly and then levels out. That is the reason why a logarithmic trendline is the best-fit curved to describe the evolution of the bubble volume as the mesh becomes more refined. So, it is proved that at a certain point in the graph, bubble's volume remains almost the same. For example, in the cases of 4g and 8g, where the volume is considerably smaller than for 1g, the ceiling of the volume value it is nearly reached for 150000 cells, while 1g's plot does not get close to the maximum value since approximately 300000 cells. However, it is clearly showed that as the number of cells increases, the volume value obtained is more accurate.

The same study was done for the rise velocity, due to it is the other magnitude of interest in this project. The figure 4.3 contains the results of the corresponding simulations:

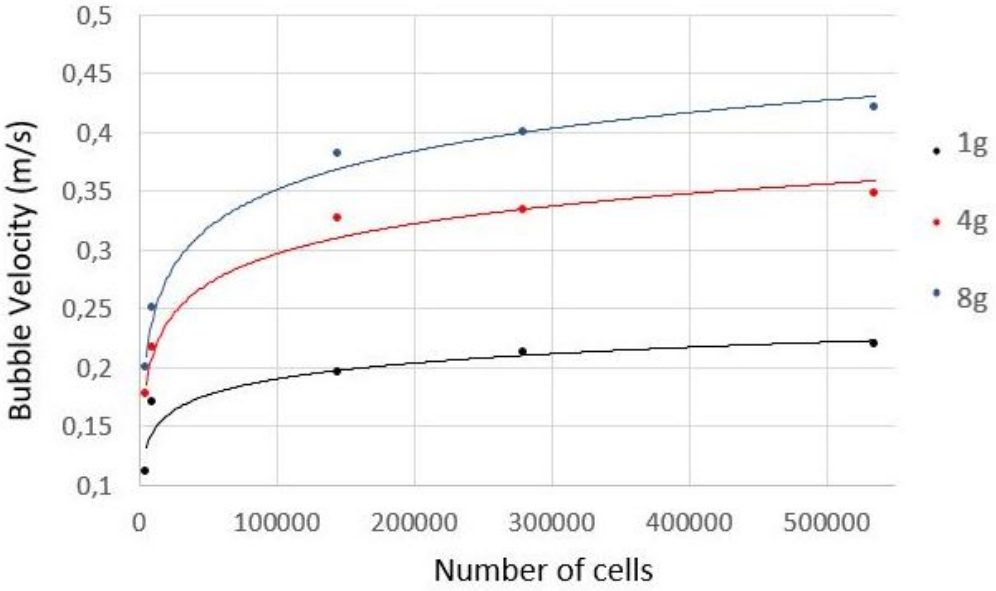

Figure 4.3: Bubble rise velocity as a function of the number of cells for different gravity levels at $U_{sg} = 0.06m/s$.

In the figure 4.3 it can be appreciated a similar plot for each gravity considering the ones obtained measuring the volume. Just like in the previous figure, a logarithmic trendline has been used as it is the best-fit curved to describe the velocity results, but, still, it is an approximation to the data obtained. Furthermore, some differences can be contrasted considering also the volume results. The velocity graphs are closer between them than the previous ones, since the values resulting from the measured magnitude are more similar. Besides, the increase of the velocity is more abrupt initially and more prolonged as the number of cells increases, although the variation of the ordinate axis is much smaller than in 4.2. Therefore, it could be stated that from the value belonging to 280000 cells, the bubble rate of ascent begins to stabilize, given that the difference between this and the rise velocity corresponding to 500000 cells is very small for all the gravity levels.

Even though it is not the goal to study neither in figure 4.2 nor in 4.3, it can be seen that the for 8g simulation the bubble volume is the smallest one, although the obtained for 4g is relatively similar, but the bubbles achieve the highest rise velocity; whereas bubbles in 1g simulation are the biggest ones and also the slowest, in relation to the resulting bubbles in 4g and 8g. In the table 4.1 are shown the results regarding the error percentage of the velocity and volume that are analysed in this mesh convergence study:

Table 4.1: Error percentage compared to the most refined mesh.

Number of cells	V_B at 1g	V_B at 4g	V_B at 8g	U_B at 1g	U_B at 4g	U_B at 8g
5000	15.52%	16.38%	29.79%	46.32%	48.89%	47.22%
10000	12.24%	4.09%	10.64%	22.34%	37.84%	40.63%
140000	6.87%	0.79%	0.43%	10.98%	8.00%	9.52%
280000	1.79%	0.47%	0.20%	2.92%	4.17%	5.00%
535000	-	-	-	-	-	-

The table 4.1 completely clarifies the need to test and study the mesh convergence. As it can be observed, the Δx of the grid is essential to get the best results possible. From the table above, it is proved that the more dense is the mesh the less error is obtained, taking as a reference the 535k mesh that is the most refined one. For example, the case of bubble volume at 1g for 5k cells overtakes by more than double the error resulting from the 140k mesh at the same gravity level. However, for other g's but measuring the volume also, there are bigger difference in terms of percentage error. For the velocity measures, there can be appreciated larger errors than for the volume results. Also it can be affirmed in general terms that the error increases as the gravity level increases. From the velocity measurements, can be seen that the errors obtained for the coarsest mesh are approximately ten times larger than the ones from the 280k tests.

Despite a denser grid will get more accuracy in the results, a bigger number of cells implies more computational time. For instance, a simulation of the 535k cell mesh could take around 150 hours, while for the mesh of 280k cells the computational time was reduced to 60 hours. Therefore, in order to choose the better mesh for the simulations it is required to find an equilibrium of correctness and efficiency for the computational performance. Considering the results showed in both figures and in table 4.1, it was selected the mesh with a total number of cells equal to 280000 since it attained very similar percentage errors in comparison with the better grid, in addition to requiring a considerable lower computational time for the simulations. Lastly, it is important to mention that this specific mesh ensures a maximum volume error of 2%, and a maximum velocity error of 5%, which are very acceptable limit values to validate accuracy in the results of this project.

4.3. Time step convergence

The analysis of the simulations time step (Δt) is strongly related with the mesh convergence. Both studies have as main goal developing the most efficient simulation capable of computing the better results within the limits established by the computer used. This variable has a key role because is the one responsible of temporal accuracy and numerical stability of the simulation, as it has been explained in 1.2.2..

In the same way as for the mesh convergence analysis, to ensure accuracy and efficiency, multiple simulations were performed changing the Δt. So, in this study it is validated the variation of the bubble volume and rise velocity values because of the time step, and also the relative error obtained for each Δt as the gravity is increased.

This tests were attempted to be performed by the standard time step used for the mesh convergence simulations: $6.5 \cdot 10^{-6} s$, and then for different values going from $\Delta t/2$ to $10 \cdot \Delta t$, passing through $2 \cdot \Delta t$ and $6 \cdot \Delta t$, considering $\Delta t = 6.5 \cdot 10^{-6} s$. This standard value was taken from an option offered by OpenFOAM called *adjustTimeStep*, which allows to adjust the time step in each iteration so that the Courant number stays within its desired range of values for a better simulation's performance. Additionally, it must me remarked that before starting with the simulations, the Δt values for the tests were checked with the ones used in [5].

However, in spite of this tests it was needed to change some of the time step values chosen, specifically: $6 \cdot \Delta t$ and $10 \cdot \Delta t$. This was decided because when the simulations were executed with the biggest time steps, OpenFOAM's simulations stopped due to an uncon-

trolled increased of the Courant number (check the explanation in 1.2.2.). Furthermore, only one test was done with the passage of time smaller than the standard, because it was checked in the previous validation study, for the mesh of 280k cells with $\Delta t = 6.5 \cdot 10^{-6} s$, that the computational time used for the simulation was notorious. Therefore, each small reduction of the time step would increase significantly the computational time, which would slow down this process. For example, by reducing the Δt from $6.5 \cdot 10^{-6} s$ to $3.25 \cdot 10^{-6} s$, the computational time, in the worst-case simulation that corresponds to 1g conditions as it is the slowest one, could increase approximately from 60 hours to 130 hours.

The simulations for the time step convergence validations were run with the following setup parameters: $U_{sg} = 0.06 m/s$, $\varnothing_c$ =0.001 m , h_v =0.022 m, $\varnothing_v$ =0.0035 m and a mesh made up by 280k cells. Finally, the time steps selected for this analysis were: $3.25 \cdot 10^{-6} s$, $6.5 \cdot 10^{-6} s$, $1.0 \cdot 10^{-5} s$ and $1.3 \cdot 10^{-5} s$. Even so, there were some problems with the largest Δt simulation for 1g, as it took the largest time to generate bubbles and Courant number was increasing more and more until at a certain point the simulation stopped. That is why in the figure 4.5 and in the table 4.2 where are showed the results, there is no measure of the rise velocity for 1g. Then, it was decided to include the test for $\Delta t = 1.0 \cdot 10^{-5} s$, with the intention to show more evidently the evolution of the results obtained.

The figure 4.4 shows the difference in the bubble volume computed depending on Δt parameter. The results obtained from the corresponding simulations can be seen in the figure below:

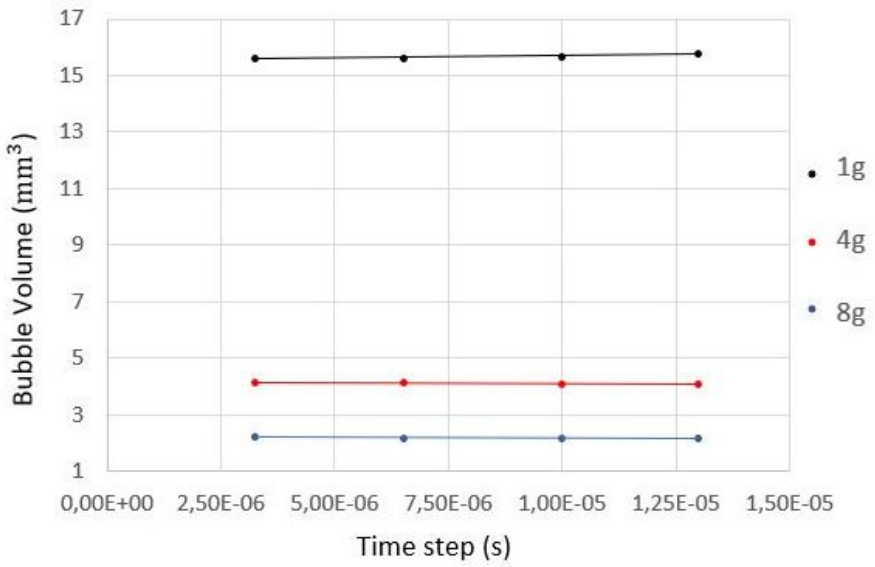

Figure 4.4: Bubble volume as a function of the time step for different gravity levels at $U_{sg} = 0.06 m/s$.

From figure 4.4, it can be observed that the measured volumes for each gravity hardly vary as the plots are approximately horizontal straight lines, which could mean that since the difference between the time step values defined is very small, the influence on volume's value degradation due to this parameter can't be checked clearly. The main limitation responsible of hampering bubble's volume evolution analysis depending on Δt has been Courant's number trouble mentioned before. Thus, the main conclusion taken from this figure is that the size of the time step values allows for achieving enough accuracy in the

results, as the difference between these and the ones from 4.2 is insignificant, and besides, the computational time required by the simulation is reasonable for this project.

As in the previous section about mesh convergence, the same study was done for the rise velocity. In figure 4.5 can be checked the resulting plots:

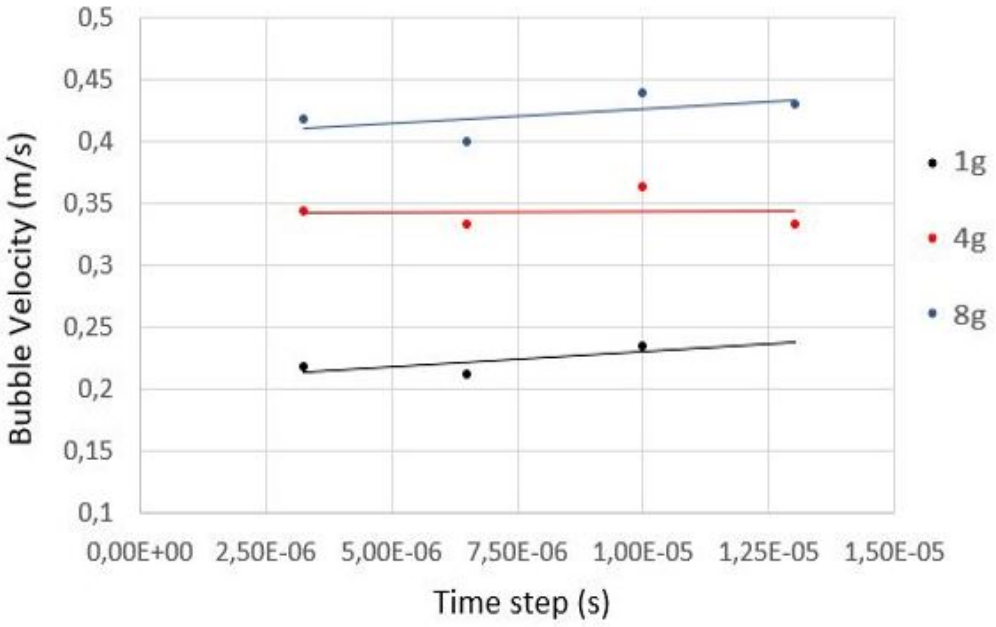

Figure 4.5: Bubble rise velocity as a function of the time step for different gravity levels at $U_{sg} = 0.06m/s$.

From 4.3 it can be appreciated again similar plots for each gravity comparing them to the bubble volume graphs. However, in this figure there is more dispersion in the velocity values measured for each gravity level. Like in figure 4.4, it can be said that the information showed is not enough to make a statement about the evolution of bubble's rise velocity as a function of Δt, but it has been accomplished the validation in terms of correctness, since the values for the smallest time steps are very similar to the ones corresponding for the mos refined meshes; and efficiency, as the computational time needed for the simulations is quite moderate.

In the table 4.2 are shown the results regarding the error percentage of both volume and velocity and that are analysed in this time step convergence section:

Table 4.2: Error percentage compared to the smallest time step.

Time step (s)	V_B at 1g	V_B at 4g	V_B at 8g	U_B at 1g	U_B at 4g	U_B at 8g
$1.3 \cdot 10^{-5}$	1.02%	1.54%	1.58%	X	5.95%	6.09%
$1.0 \cdot 10^{-5}$	0.33%	1.08%	0.95%	7.44%	5.73%	6.22%
$6.5 \cdot 10^{-6}$	0.31%	0.37%	0.36%	3.12%	3.04%	4.31%
$3.25 \cdot 10^{-6}$	-	-	-	-	-	-

From the table 4.2 it can be observed that the Δt of the simulation has impact in the correctness of the results obtained, despite it was attempted to test a wider range of values

to highlight the impact of this parameter. Unlike in table 4.1, as the results for the time step convergence validation have been more similar for each gravity case, it can be seen a smaller percentage error spread along the table. The most evident conclusion that can be drown watching the evolution of percentage errors is that the smaller is the time step, the less error is obtained in the parameter's value measured. Excepting this statement, it is not possible to determine any other conclusion, since this error does not develop following tendency with the increase or decrease of gravity.

Finally, considering the results analysed and the requirements of efficiency and accuracy to accomplish, $\Delta t = 6.5 \cdot 10^{-6} s$ has been defined as best time step. Even though it would have been wanted to test some more Δt values, with the ones used for these simulations it has been enough to check that for $6.5 \cdot 10^{-6} s$ were achieved very correct results, as well as the computational time would not hinder the project's schedule. In particular, for this time step it is ensured that the maximum error in bubble volume results is of 0.4 % and regarding rise velocity measures the error will not exceed 4.5 %. A deciding indicator to know that it has been analysed correctly this parameter is the fact that when a simulation is running with the option *adjustTimeStep* activated, the range of values chosen automatically by OpenFOAM oscillates around $6.5 \mu s$. However, it has been considered that the best simulation's performance would be achieved letting OpenFOAM adjust the time step to keep inside the bounds the Courant number.

4.4. Influence of the transient

The interest of this analysis is to validate from which bubble can be done the volume and velocity measurements without the results being altered by the transient phenomenon. For this project, the transient concept is referred to the difference between the first bubble generation time and the subsequent ones. This event happens because the first bubble starts its formation process from scratch, so the gas injected from the capillary has to fight against the surface tension forces of the static liquid inside the volume, otherwise the bubble would not be generated. However, the following bubbles do not start the formation process from zero, since at the detachment stage of the previous bubble it is leaved a remaining part in the injection area. The figure 4.6 contains two captures of the bubble's formation start, in the left side for a first simulated bubble and next to it the one representing any subsequent bubble.

Figure 4.6: Capture of the transient event along bubble formation.

As commented before, this figure clearly shows the difference between the first stage of the bubble formation for each case. On one hand, it can be appreciated the remaining gas left in the lower wall when the previous bubble has detached, which signifies that the following bubble would take less time until it detaches. On the other hand, the capture on the left shows the interphase separating the liquid from the gas, which has been injected from the base.

Therefore, the interest of studying the transient lies in understanding how the bubble volume and rise velocity measures are affected, considering that in any system where a fluid problem like this occurs, the global behaviour of bubbles will not be represented by the first one, but from which the behaviour of the following bubbles remains the same.

The results obtained for the corresponding tests are showed in the following figures. In figure 4.7 can be seen the evolution of the bubble volume and rise velocity depending on the order of the bubble's generation:

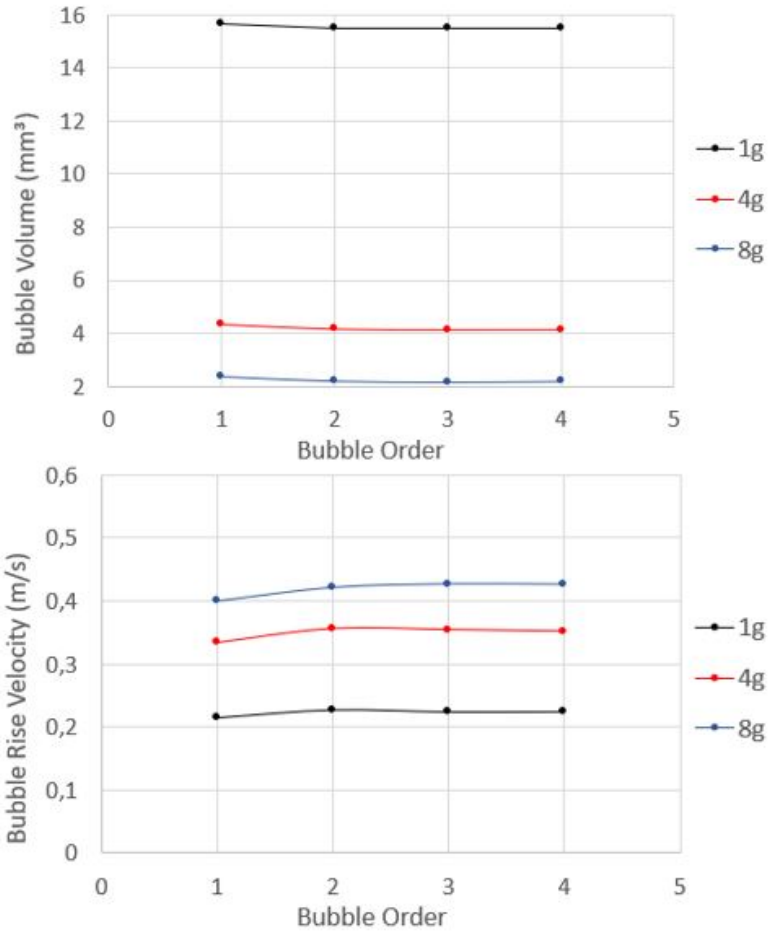

Figure 4.7: Bubble volume and rise velocity for different bubbles of the same simulation.

As it can be deduced, the total number of bubbles generated in that simulation, and most of the simulations in other tests, was four. The reason why are generated only four bubbles is mainly because the simulation's computational time is quite high, and 4 is considered a reasonable amount since the volume and velocity values vary very little from the second bubble. For instance, if the time required to generate one bubble and let it rise is around 35-40 hours, in the worst scenario (1g conditions), the subsequent bubbles would take a

similar amount of time so that the computational time would be increasing proportionally. Regarding the figure 4.7, for both magnitudes' results it can be appreciated that from the second measure (for all gravities) the graph stabilizes, which implies that the values of each magnitude measured for the following bubbles are very similar to the preliminary ones. The only fact important to remark is that the plots of the volume start decreasing before the stabilization, whereas the rise velocity firstly increases and then stabilizes. This makes sense as the first bubble starts the formation from zero which induces more time of growth up to the detachment and then a bigger volume, that at the same time can imply a little smaller rise velocity.

Furthermore, it has been compared the relative error between each bubble with the last one, in this case the number four, with the objective of proving from which bubble it can be considered that the measure is good enough regarding the best result, that corresponds to the last bubble generated. The figure 4.8 shows the relative error of the first, second and third bubbles with the last one for both magnitudes:

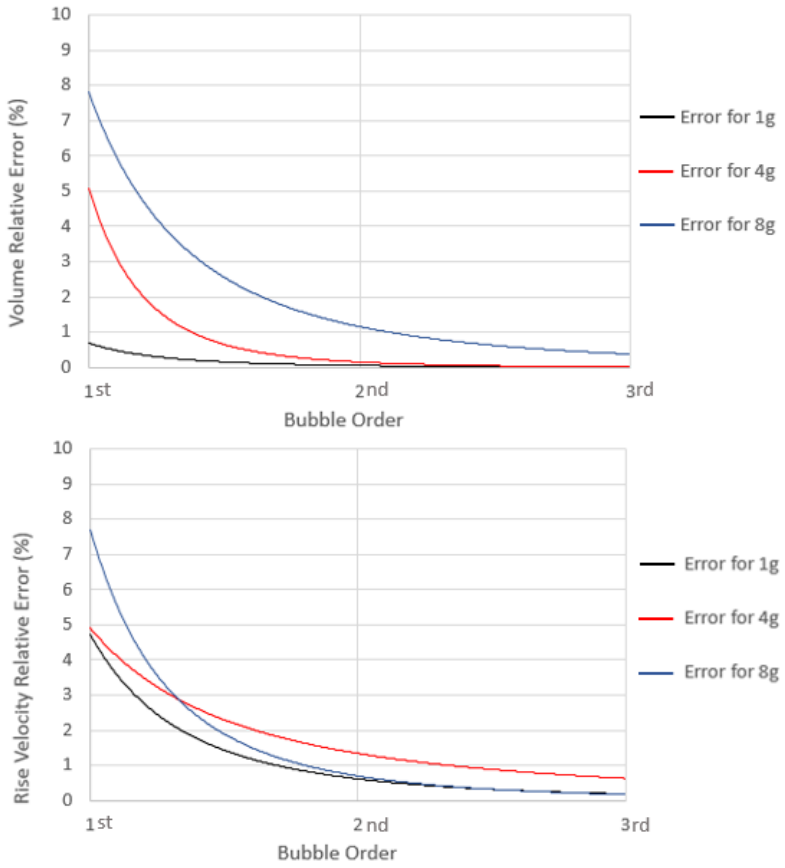

Figure 4.8: Relative errors in volume and rise velocity results for different gravity levels.

From this figure it can be said that for all the cases of each magnitude, there is an important decrease of the relative error from the first bubble to the second. Just for the volume measures it can be stated that 8g is the case with the biggest errors and 1g the opposite. The most important information from these two graphs is that for both volume and velocity results, the errors obtained in the third bubble are always smaller than 1 % , so the value can be considered almost equal to the one obtained in the last bubble. Therefore, it could be stopped the simulation after the third bubble and the results obtained would be less

than 1 % different to the ones corresponding the the subsequent bubble, while at the same time it would be reducing the simulation time in a quarter.

4.5. Bubble formation process

In this section it is going to be studied the bubble formation process obtained by means of simulations injecting air at $U_{sg} = 0.06m/s$. The objective is to validate that after the gas is injected into the liquid from the base of the tube, the bubble generated behaves as it corresponds during the formation process. Once validated this, the formation in normal gravity is going to be compared with the same process when the fluid is under five times the gravity on Earth.

Ying et al. studied in [20] the characteristics of bubble motion on rising process. They divided the formation process in two different stages: growth and detachment. Figure 4.9 shows the formation process obtained in the mentioned report where it can be seen how the bubble grows, in the first and second images, and the detachment stage, in the second and third images:

Figure 4.9: Growth and detachment stages of bubble formation.

In [20], it is determined that during the growth stage, the bubble radius increases rapidly based on orifice size. Regarding the vertical development, the bubble mainly grows, and besides stretches lengthwise, due to the impact of the gas injected. Moreover, the bubble gently grows into a smooth ellipsoid shape governed by surface tension forces. It can be observed that as the bubble grows the horizontal coordinate of bubble's center of mass remains unchanged, whereas the vertical position moves up. Lastly, near the detachment from the solid wall, the area of the bubble's neck decreases gradually while the center of mass remains at the same axial position.

First of all, it is going to compare the case in [20] with the simulation's results for the same conditions. So, as the previous experiment was performed in normal gravity conditions, the same gravity was defined in OpenFOAM. In figure 4.10 it is compared bubble's outline along its formation for the same instants of time. The left side is a capture of the bubble's development corresponding to [20], while in the right side it can be appreciated the formation of a simulated bubble.

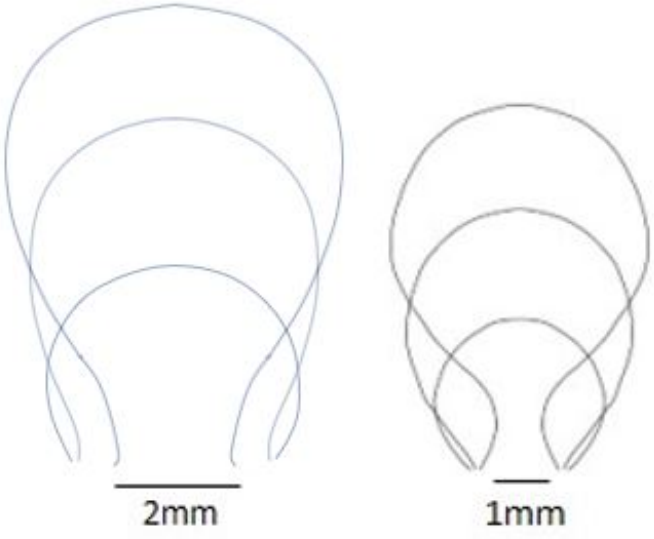

Figure 4.10: Outlines of the bubbles during the formation process.

Observing figure 4.10, it can be verified that during the bubble's growth, there is an important increase of its volume. Besides, it can be seen in the plot how the bubble gradually takes a smooth ellipsoid shape, as it happened in the other case. Regarding the center of mass, it can be checked from the right graph in figure 4.10 that the abscissa coordinate remains the same during the formation process, while the vertical one moves up in accordance with the bubble's development. Furthermore, from the simulation case it can be seen that the contact area with the solid wall does not reduce as much as in the first case, which could be due to a difference in the hydrophilic properties of the solid material. Therefore, the simulated solid would be more hydrophobic since the bubble spreads much less on the surface than in [20]. The last aspect that can be validated is the gradual reduction of the bubble neck during the detachment process. So, it can be concluded that despite the difference in orifice diameter, which clearly affects to the bubble's size, the behaviour of both bubbles throughout the formation process is almost the same.

Once it has been proved that the formation process unfolds as expected, it can be analysed the gravity effect in this phenomenon. For this, it were performed two simulations, but instead of both for Earth's gravity conditions, in one it was set a value five times bigger than the standard. This was done with the objective of understanding how gravity affects the bubble formation process. The following figure contains two graphs, the left one corresponds to 1g simulation and the other to 5g:

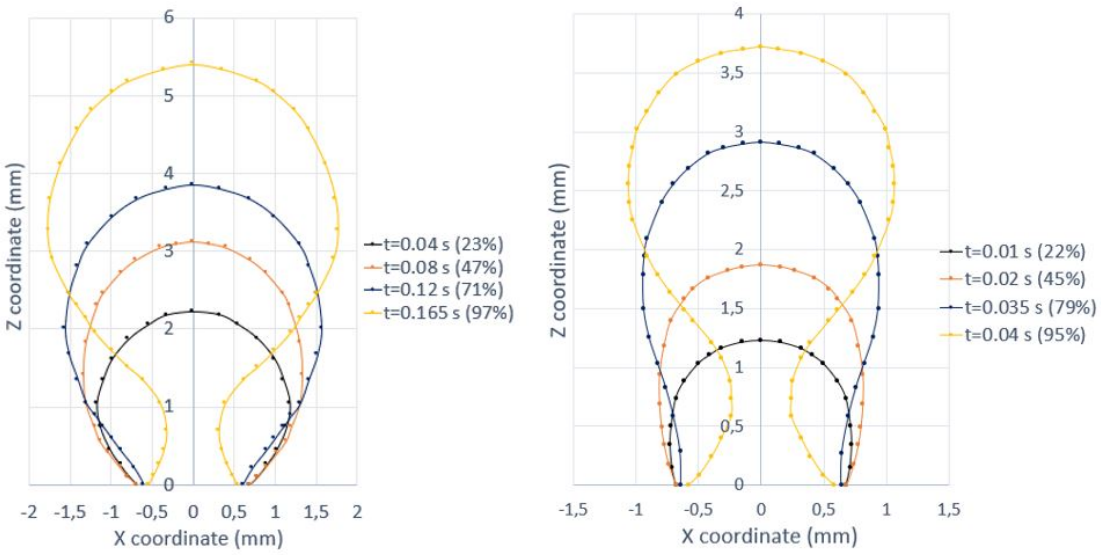

Figure 4.11: OpenFOAM's bubble formation for 1g and 5g.

It must be noticed that in figure 4.11 there is a legend for each graph giving information about the time passed for any bubble plot and the percentage of formation relative to the total formation time of each bubble. As for the time of bubble formation (before the detachment), there is a significant difference between both cases. While the bubble for hipergravity conditions is generated in 0.04 s approximately, for Earth gravity takes around 0.17 s. Another notable difference is the shape of the bubble during the different stages of formation. As it can be appreciated in 4.11, during growth stage for 5g, the bubble has more elongated shape, as if it was being stretched upwards.

From figure 4.11 it can be also checked the differences of size and shape between both bubbles in four different points of the formation process, although the evolution along the growth and detachment stages is similar for 1g and 5g. Taking into consideration all the observations, it can be concluded that the fact of increasing gravity produces a pull up effect on the bubble, which in turn, speeds up its formation process. This event comes from the buoyancy force, defined as: $F_b = \rho_l V_b g$. In fact, the Bond number represents the buoyancy force divided by the surface tension force. Hence, when gravity is increased, the buoyancy force and Bond number increase as well, and then the bubble is stretched upwards. To finish the bubble formation analysis, it must be remarked a last fact related with the size of the bubble. On the left side graph, the bubble achieves a height near 5.5 mm and a width around 3.5 mm, while the bubble subjected to hypergravity measures approximately 3.75 mm of height and 2.5 mm of width. So it can be concluded that as the gravity increases, the bubble volume is smaller, since the buoyancy effect forces an earlier detachment of the bubble and therefore it has less time to grow.

CHAPTER 5. RESULTS AND DISCUSSION

This chapter will discuss the results obtained from the OpenFOAM's simulations along this project. In addition to the analysis, the results will be also compared with the experimental data from [1]. After the validations performed in the previous chapter, it can be assured a correct behaviour of the bubbles in both formation process and rise path, and also that the results presented below meet the defined accuracy criteria.

For all these simulations have been set the physical properties of distilled-water and air commented in 3.3.3., as well as the 280k cells mesh, the time step option *adjustTimeStep* corresponding to $\Delta t = 6.5 \cdot 10^{-}6s$ and the contact angle $\theta = 25^{o}$, all these validated previously in 4. Furthermore, all the volume and velocity measures for each gravity has been done for the third bubble generated in the simulation, as it has been proved in 4.4. that the volume and velocity values are stabilized.

Figure 5.1 shows the rising bubbles obtained with OpenFOAM's simulations in contrast with the ones captured in [1]. Besides, the ascent has been studied for different gravity levels to observe the differences between them.

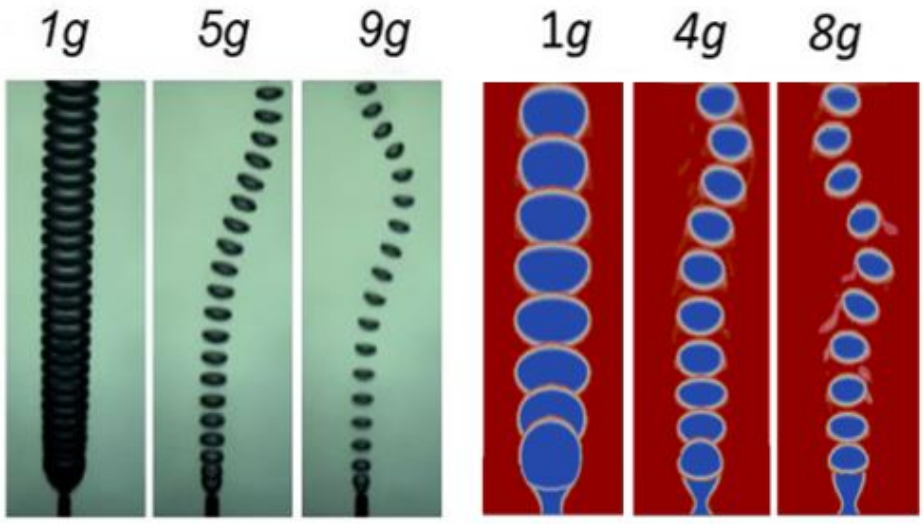

Figure 5.1: Bubble rise comparison between experimental results (1st column) and simulations (2nd column).

At first sight, it can be appreciated that bubbles simulated behave in the same way as real ones. As gravity increases, there are two main features that can be observed qualitatively from the figure: the first one is that bubble's size decreases; and the second characteristic is that in both experiments at 1g conditions the bubble rises straight up, but when gravitational effects are increased, the bubble oscillates laterally with a zig-zag motion and with increasing oscillation frequency. So, from this figure it can be said that the simulation's results are satisfactory since it is achieved a bubble behaviour like in the reference experiment, not only at normal gravity but also for hypergravity conditions. Although the results seem right qualitatively, the volume and the rise velocity were measured in order to analyse quantitatively the CFD results in comparison with the experimental ones. These

magnitudes are presented with the corresponding numerical data in the following sections.

5.1. Path Transition

Up to this part of the project it has been studied in great detail the bubble formation process, but in this section, it will be analysed the bubble's vertical ascent. Specifically, the type of trajectory will be related with the gas injection velocity, that at the same time affects the bubble volume.

The interest of studying the path transition event emerged while checking a simulation. As this project is based in [1], it was expected the zig-zag path after the straight ascent, but when the rising bubble left the 2D vertical plane, it was conjectured that the trajectory could have another stage corresponding to a 3D motion, which was definitely confirmed.

Shew et al. carried out a research [9] about forces acting on rising bubbles. It was proved that the rise path can have different types of trajectories, not only the vertical straight one, but also a zig-zag or an helicoidal path. In fact, one of the most interesting results extracted from that study is the path type transition along the rise, as it can be seen in figure 5.2.

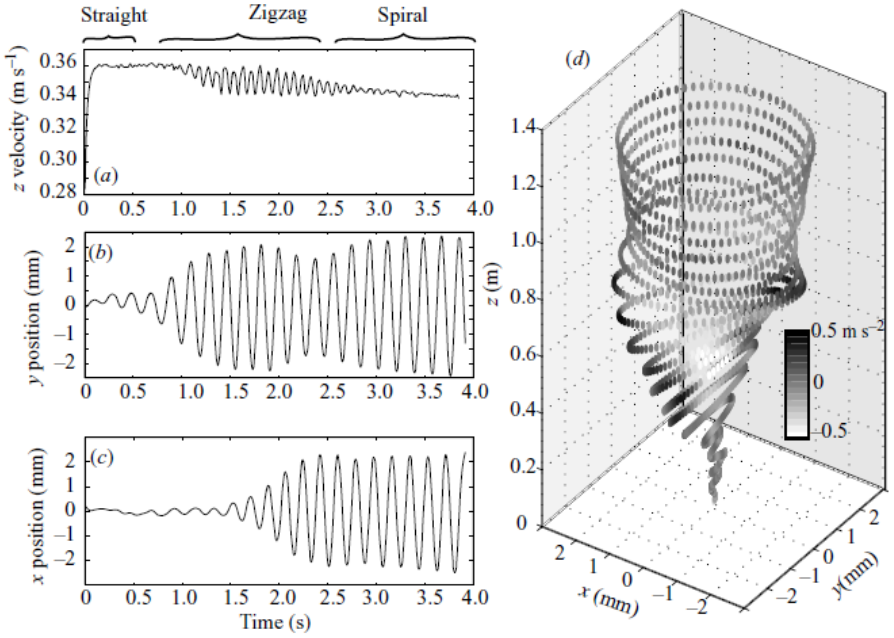

Figure 5.2: Example of bubble trajectory. a) Vertical component of velocity, (b) y position from camera data, (c) x position from camera data, and (d) three-dimensional reconstruction of full trajectory.

From the figure 5.2 it can be seen that the bubble begins rising straight, followed by a zig-zag path in the y-z plane, and finally a 3D spiral motion with a steady rise velocity. This results show clearly the different stages of a bubble trajectory for normal gravity.

Still, this experiment was conducted in a container much higher than the tube simulated with OpenFOAM, which means that most of the bubble path evolution is not observed. Nevertheless, as the study carried out in this project contemplates different gravity levels, from 1g to 9g, it will be showed that this event takes place much closer to the base.

Therefore, several simulations were run to achieve, for each gravity test, the U_{sg} from which

the trajectory, after the vertical straight rise, passed to helicoidal motion instead of zig-zag. In figure 5.3 can be seen the results obtained for this section:

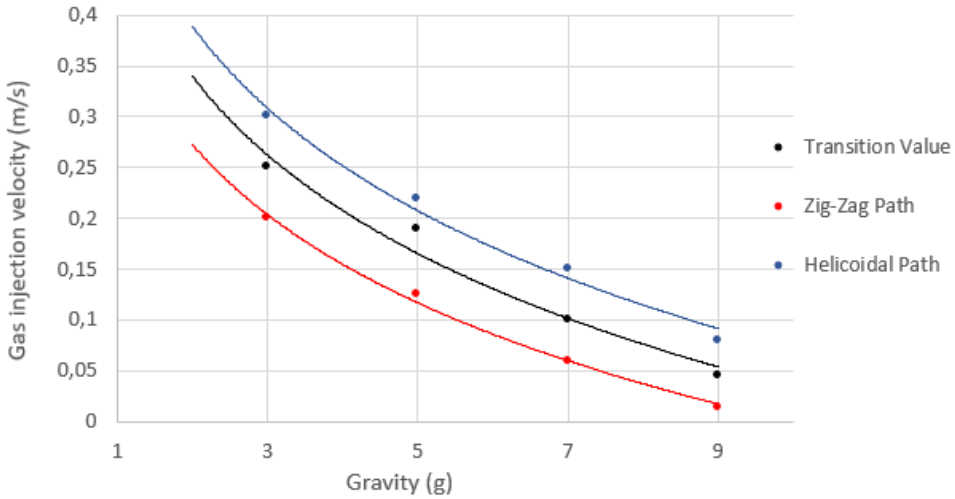

Figure 5.3: Trajectory transition of the bubble regarding U_{sg} for different gravity levels.

In figure 5.3 are shown graphically the results obtained varying the gas injection velocity at different hypergravity conditions. As in previous graphs, it has been used a trendline well-fitted to the data obtained, in order to describe approximately the evolution of the trajectory with the gravity level. The black plot represents trajectory transition cases for a specific U_{sg} and the corresponding gravity. This line pretend to determine the point from which if it is increased injection rate, the path changes from zig-zag to helicoidal motion. Since it would be required a very large number of simulations to achieve this exact transition point, it was decided to plot also, for each gravity tested, the values that would ensure zig-zag trajectory (red line) and helicoidal trajectory (blue line). So it can be stated that above the blue plot the bubble would rise following a 3D ellipsoidal motion, whereas under the red plot bubbles rise drawing a zig-zag path. Therefore, the area contained between these two lines would represent a range of values for which the bubble is in a transition process, considering some margin in both sides of the black line. Additionally, it is important to remark that all these results and statements are subjected to the height of the cylinder simulated for the study, since probably for larger heights the zig-zag trajectory would end up developing as helicoidal.

From the figure it can be appreciated that as the gravity level increases, the smaller gas injection velocity is required to achieve the zig-zag motion of the bubbles. For example, the zig zag area for 3g goes up to $U_{sg} = 0.2m/s$ and the 3D motion starts from around $0.3m/s$, while for 9g the 2D oscillation zone ends considerably sooner: $U_{sg} = 0.05m/s$, and the helicoidal trajectory zone starts approximately from $0.09m/s$. So, it can be concluded that gravitational forces have a several impact to the type of trajectory in rising bubbles, since they are more destabilized for higher gravity conditions. As it is proved in the graph above, this event can be compensated by reducing the injection velocity of the air to generate gently the bubble.

5.2. Analysis of bubble volume and rise velocity

At this point, it has been defined: the mesh, time step, contact angle, from which number of bubble can be trusted both volume and rise velocity measures, and lastly, with the path transition study it is known for which U_{sg} (at different gravity levels) the trajectory followed by bubbles is a zig-zag path. Considering the last one, the gas injection velocities were selected for these final tests. From figure 5.3, the U_{sg} values for each gravity that belonged to helicoidal path area were disregarded, as the bubbles' trajectory obtained in [1] were zig-zag. So, the chosen injection velocities for the volume and velocity final tests are: $0.03m/s$, $0.06m/s$ and $0.1m/s$. In the mentioned figure can be checked that these velocities are below the helical trajectory plot for all gravity conditions. The objective of this section is to study how the gravity affects to the volume and rise velocity of bubbles. Besides it was decided to perform the tests for different U_{sg} in order to analyse also the influence of the gas injection rate in these magnitudes for hypergravity conditions.

The simulations in this section have been performed for 1g, 2g, 4g, 6g and 8g, to obtain an accurate graph of volume and rise velocity evolution, as these results will be compared with the theoretical equations (5.1 and 5.3) used in [1]. The bubble equivalent diameter is defined by:

$$d_{eq} = \left(\frac{6\sigma\varnothing_c}{\rho_l g} \right)^{\frac{1}{3}} \tag{5.1}$$

From the equivalent diameter can be obtained the bubble volume:

$$V_b = \frac{4}{3}\pi \left(\frac{d_{eq}}{2} \right)^3 \tag{5.2}$$

On the other hand, the rise velocity of the bubble is expressed as follows:

$$U_b = \left(\left(\frac{4\sigma^2 g}{3\rho_l^2 g} \right)^{\frac{1}{3}} + \left(\frac{3\sigma\varnothing_c g^2}{4\rho_l} \right)^{\frac{1}{3}} \right)^{\frac{1}{2}} \tag{5.3}$$

Once the equations are presented, it can be continued with the presentation of the results. For the specified fluids, d_{eq} and U_b depend, according to equations 5.1 and 5.3, on gravity only. Hence the horizontal axis in the following graphs is the gravity level. Firstly, the bubble volume graphs are showed in figure 5.4. The one above represents the values measured in comparison with the equation 5.2 and the other represents the relative error of the values corresponding to each U_{sg} with the theoretical plot:

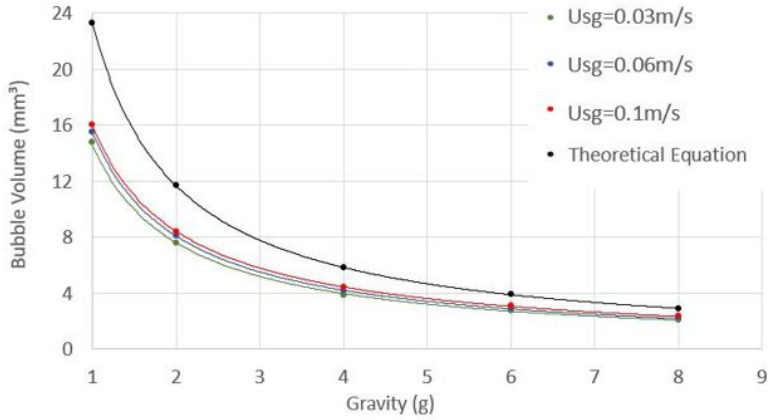

(a) Bubble volume evolution related with the gravity level.

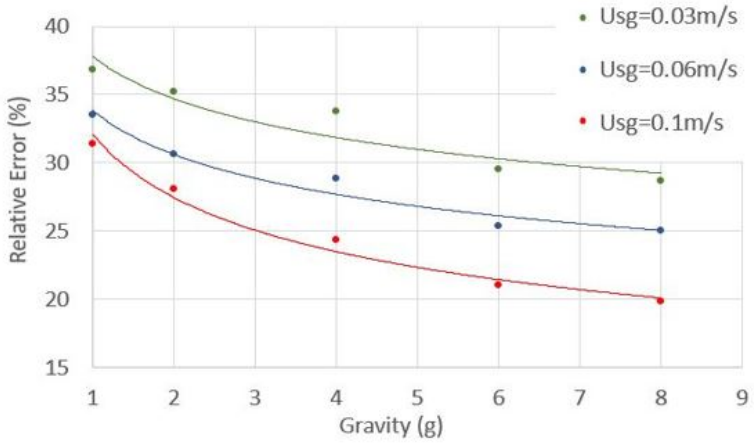

(b) Relative error of OpenFOAM's values regarding the theoretical equation.

Figure 5.4: Bubble volume for different gas injection velocities.

The curves in figure 5.4(a) correspond to the analytical model 5.1 previously presented. Regarding the volume, figure 5.4(a) corroborates the potential decrease of the bubble volume as the gravity increases, which was detected in the previous chapter. Moreover, for higher gas injection velocities the volume of the bubble increases, without changing any other conditions, although for the different U_{sg} tested the variation of the value is really small. Also from 5.4(a) it can be appreciated how the volume decreases very fast initially, but then stabilizes gradually until approaching to a horizontal line. With respect to the theoretical plot, there is a significant difference between this one and the three plots obtained from the simulations.

In order to measure the error made in OpenFOAM, it was done the second graph 5.4(b). It can be checked that the simulations with less error in relation to the equation are the ones performed for $U_{sg} = 0.1m/s$, unlike $U_{sg} = 0.03m/s$ simulations that have higher percentage error. Furthermore as the gravity increases, the error made in the numerical analysis decreases. For example, the better case shows the percentage is reduced from 31% to 20%.

The same studies were performed for the other magnitude of interest, the rise velocity of the bubble. The corresponding results are showed in figure 5.5:

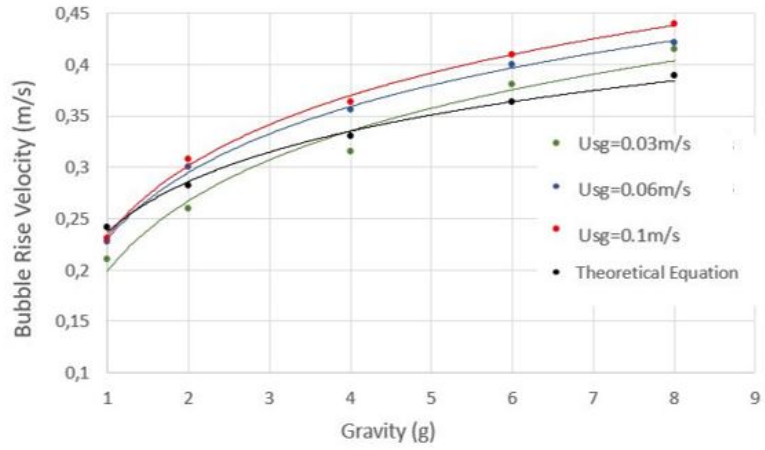

(a) Bubble velocity evolution related with the gravity level.

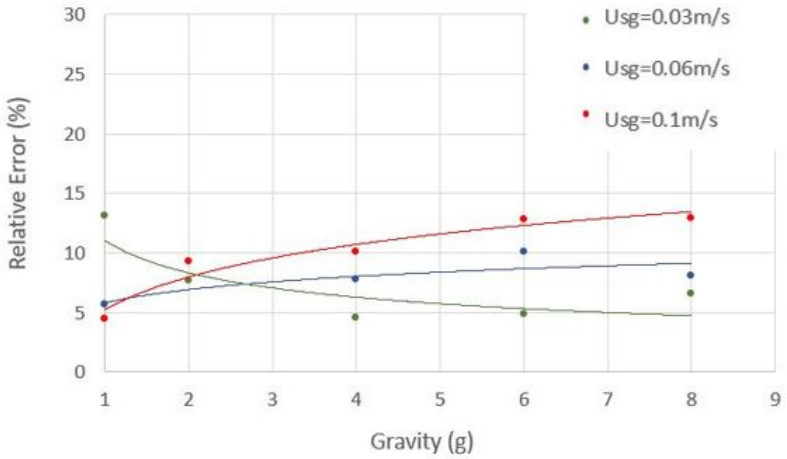

(b) Relative error of OpenFOAM's results regarding the theoretical equation.

Figure 5.5: Bubble rise velocity for different gas injection velocities.

For the velocity results, the curves used in figure 5.5(a) correspond to the analytical model 5.3 presented at the beginning of this section. From figure 5.5(a), it can be stated that the bubble velocity increases as the gravity increases, which was also seen in the previous chapter. The evolution of this magnitude certainly follows a continued increase, but more notable for lower gravities. Furthermore, it can be perceived that the gas injection velocity has influence in the rise velocity, since for bigger U_{sg} the plot is higher up in the graph, which means faster ascents. Regarding the difference between the theoretical equation curve and the other three obtained trough the simulations, it can be observed that the results in the figure 5.5 are more similar to the analytical model than the ones showed in figure 5.4. At 1g the three cases are under the theoretical value, but as the gravity level is increased, these curves surpass the one corresponding to the equation 5.3.

The same way than before, the relative error obtained in the simulations regarding the theoretical equation can be seen in 5.5(b). In this graph there is a significant decrease of the error in comparison with 5.4(b), as the largest percentage does not reach the 15%. From this figure can be noticed that the higher U_{sg} has an increase tendency of the error despite at 6g the curve starts stabilizing. The intermediate gas injection velocity is the most constant as the error is maintained from 5% to 10% throughout the different gravities

and it shows that the results achieved are better than for $0.1m/s$. Lastly, the best error curve is the one corresponding to $U_{sg} = 0.03m/s$, which despite starting with the highest percentage 13%, tends to decrease since it is achieved the stabilization around 5%.

CONCLUSIONS

This study reproduces with CFD software OpenFOAM v6.0 the experiments done in the ESA's LDC, where a bubble column was generated by connecting a millimetric capillary gas injector to the base of a vessel filled of distilled water. So, by means of simulations, the numerical results have been obtained to compare the virtual experiment with the previous one.

Before carrying out the final tests, some validations were done to assure the simulation's set-up parameters, the bubble formation process and the transient's influence on the bubble generation, in which it would be analysed the magnitudes of interest to compare them with the results in [1]. The mesh convergence analysis shows that a grid of 280k cells is enough to achieve the accuracy desired and an efficient computational time, just like with $\Delta t = 6.5 \cdot 10^{-6} s$ in the corresponding time step convergence test. Furthermore, the contact angle study proves that the hydrophilic properties of the solid walls affects significantly to the behaviour of the bubble throughout its formation from the capillary, and it is observed qualitatively that for $\theta = 25^{o}$ the simulated bubble behaves like the one obtained from the millimetric syringe in the LDC experiment.

The final simulations were performed after these validations. From the path transition study it can be stated that the bubble rise is easily destabilized by gravity, which takes the trajectory from a zig-zag to an helicoidal motion. This effect can be compensated by regulating the U_{sg}, so as gravitational effects increase, the vertical ascent of the bubble is more destabilized and it is required to reduce the gas injection rate to keep bubbles drawing a zig-zag path. Then, three different gas injection velocities were tested within the boundaries of this 2D trajectory: $0.03 m/s$, $0.06 m/s$ and $0.1 m/s$, and at different gravity levels, from 1g to 8g. The bubble volume and rise velocity are measured parameters that have been compared and studied. The conclusion obtained once analysed the results of both magnitudes is that the numerical study is really similar to the experimental investigation, as the evolution of the two parameters in hypergravity is similar. However there are small quantitative differences coming from the difference of the capillary diameter. Therefore, the theoretical models used in [1] regarding the bubble volume and velocity were compared to the results. Observing these fittings it can be concluded that despite the similarity of the results, there is still some relative error between the equations and the numerical values, especially for the bubble volume. The error could be improved by changing some parameters, for example: increasing the contact angle to achieve more adhesion of the bubble with the surface or increasing the gas injection velocity which also leads to larger volumes. Other solutions such as refining more the mesh or reducing the time step of the simulations would require a more powerful computer, otherwise the computational time would increase considerably.

A final remark, thanks to compare OpenFOAM results with the previous ones it can be said that CFD numerical analysis has reproduced a laminar fluid flow problem successfully. In recent years, these programs have developed by leaps and bounds, which have implied an extraordinary increase of this type of investigations. But the most important thing is that this would facilitate access for future researchers to study these phenomena under hypergravity conditions.

BIBLIOGRAPHY

[1] F. Suñol and R. González-Cinca, "Effects of gravity level on bubble formation and rise in low-viscosity liquids," Physical review E.91 (5) 053009, 2015. iii, vi, 11, 12, 17, 19, 26, 28, 33, 34, 35, 47, 48, 50, 55

[2] B. Dunbar, "What is gravity?." www.nasa.gov/shuttlestation/station/microgex.html, February 2009. 6

[3] S. Deguchi, H. Shimoshige, M. Tsudome, S. Mukai, R. Corkery, S. Ito, and K. Horikoshi, "Microbial growth at hyperaccelerations up to 403,627 x g," Physical review, 108 (19) 7997-8002, 2011. 7

[4] ESA, "Hypergravity helping aircraft fly further." http://www.esa.int/Our_Activities/, 2015. 8

[5] S. Arias and A. Montlaur, "Numerical study and experimental comparison of two-phase flow generation in a t-junction," AIAA Journal 55 (5) 1565–1574, 2017. 10, 35, 38

[6] S. Arias, D. Legendre, and R. González-Cinca, "Numerical simulation of bubble generation in a t-junction," Computer and Fluids 56 49-60, 2012. 10

[7] A. Kulkarni and J. Joshi, "Bubble formation and bubble rise velocity in gas liquid systems," Ind. Eng. Chem. Res. 44 (16), 5873-5931, 2005. 10

[8] J. Hua and J. Lou, "Numerical simulation of bubble rising in viscous liquid," Journal of Computational Physics 222, 769–795, 2007. 11

[9] W. Shew, S. Poncet, and J. Pinton, "Force measurements on rising bubbles," Fluid Mech. 569, 51–60, 2006. 11, 48

[10] R. Zenit and J. Magnaudet, "Path instability of rising spheroidal air bubbles: a shapecontrolled process," physics of fluids 20 (1), 2008. 11

[11] J. Torrent, "Medida del ángulo de contacto," tech. rep., 2013. 13

[12] H. Schlichting and K. Gersten, "Boundary-layer theory," Springer-Verlag 416–419, 2017. 14, 26

[13] M. Suo and P. Griffith, "Two-phase flow in capillary tubes," Journal of Basic Engineering 86 576-582, 1964. 14

[14] K. S. Rezkallah, "Weber number based flow-pattern maps for liquid-gas flows at microgravity," International Journal of Multiphase Flow 22 (6), 1265–1270, 1996. 15, 27

[15] O. foundation Ltd, *OpenFOAM v6 User Guide*. https://cfd.direct/openfoam/user-guide, 2018. 15

[16] M. Wu and M. Gharib, "Experimental studies on the shape and path of small air bubbles rising in clean water," Physics of Fluids 14 (7), L49, 2002. 18

[17] E. Madadi and A. Passalacqua, “Cylinder mesh using blockmesh with m4 macro.” https://www.ehsanmadadi.com/cylinder-mesh/, May 2016. 25, 66

[18] O. wiki editor, “Interfoam.” https://openfoamwiki.net/index.php/InterFoam, 2018. 28, 29

[19] A. Utkarsh, *The ParaView Guide*. Kitware Inc., community ed., 2017. 29

[20] G. Ying, H. Puzhen and W. Chaoqun, “Experimental and numerical investigation of bubble–bubble interactions during the process of free ascension,” Energies 12 (10) 1977, 2019. 44, 45

[21] OpenCFD, “Openfoam download (2004-2019).” https://www.openfoam.com/download/, 28/06/2019. 61

APPENDICES

APPENDIX A. OPENFOAM

The ultimate version of this software can be downloaded for Linux, Windows and Mac from [21], where can be found a detailed explanation about how to install OpenFOAM step by step. Moreover, there are different guides to start running the program and some tutorials to follow.

A.1. OpenFOAM case

In this section it is pretended to explain more specifically each part of the different folders forming a case to show how to start with an OpenFOAM project as it has been done in the current study. As a general information for the following captures, the dimensions of the different magnitudes are represented in a vector as [kg, m, s, K, mol, A, cd], for example m/s would be defined in OpenFOAM as [0 1 -1 0 0 0 0].

A.1.1. Constant folder

Figure A.1 shows the content of *transportProperties* file, in which can be found the physical properties of each fluid phase in addition to the surface tension of both. There is also defined the *transportModel* parameter set as Newtonian since both fluids used in the simulations are considered Newtonian.

```
/*--------------------------------*- C++ -*----------------------------------*\
| =========                 |                                                 |
| \\      /  F ield         | OpenFOAM: The Open Source CFD Toolbox           |
|  \\    /   O peration     | Version:  1.6                                   |
|   \\  /    A nd           | Web:      www.OpenFOAM.org                      |
|    \\/     M anipulation  |                                                 |
\*---------------------------------------------------------------------------*/
FoamFile
{
    version     2.0;
    format      ascii;
    class       dictionary;
    location    "constant";
    object      transportProperties;
}
// * * * * * * * * * * * * * * * * * * * * * * * * * * * * * * * * * * * * * //

phases (water air);

water
{
    transportModel  Newtonian;
    nu              nu [ 0 2 -1 0 0 0 0 ] 1e-06;
    rho             rho [ 1 -3 0 0 0 0 0 ] 1000;
}

air
{
    transportModel  Newtonian;
    nu              nu [ 0 2 -1 0 0 0 0 ] 1.48e-05;
    rho             rho [ 1 -3 0 0 0 0 0 ] 1;
}

sigma           sigma [ 1 0 -2 0 0 0 0 ] 0.0728;

// ************************************************************************* //
```

Figure A.1: Transport properties file.

The *turbulenceProperties* file (Figure A.2) just describes the turbulence model in *simulationType*, which corresponds to laminar conditions.

```
/*--------------------------------*- C++ -*----------------------------------*\
| =========                 |                                                 |
| \\      /  F ield         | OpenFOAM: The Open Source CFD Toolbox           |
|  \\    /   O peration     | Version:  1.7.1                                 |
|   \\  /    A nd           | Web:      www.OpenFOAM.com                      |
|    \\/     M anipulation  |                                                 |
\*---------------------------------------------------------------------------*/
FoamFile
{
    version     2.0;
    format      ascii;
    class       dictionary;
    location    "constant";
    object      turbulenceProperties;
}
// * * * * * * * * * * * * * * * * * * * * * * * * * * * * * * * * * * * * //

simulationType  laminar;


// ************************************************************************* //
```

Figure A.2: Turbulence properties file.

The last file of constant folder is g and can be seen in figure A.3. This one only defines the gravity value, which has been changed depending on the desired simulation's conditions, normal gravity or hypergravity.

```
/*--------------------------------*- C++ -*----------------------------------*\
| =========                 |                                                 |
| \\      /  F ield         | OpenFOAM: The Open Source CFD Toolbox           |
|  \\    /   O peration     | Version:  1.7.1                                 |
|   \\  /    A nd           | Web:      www.OpenFOAM.com                      |
|    \\/     M anipulation  |                                                 |
\*---------------------------------------------------------------------------*/
FoamFile
{
    version     2.0;
    format      ascii;
    class       uniformDimensionedVectorField;
    location    "constant";
    object      g;
}
// * * * * * * * * * * * * * * * * * * * * * * * * * * * * * * * * * * * * //

dimensions      [0 1 -2 0 0 0 0];
value           (0 0 -9.81);


// ************************************************************************* //
```

Figure A.3: Gravity file.

It must be commented that it exists one folder called polymesh, inside constant folder, which contains the mesh description. As this one is generated automatically by OpenFOAM when entering the command *blockMesh* it is not added in the appendix.

A.1.2. System folder

In *controlDict* (Figure A.4) are defined different options related to the solver, time control, data writing, in addition to the boundaries for the Courant number and the time step, as the option *adjustTimeStep* is enabled.

```
/*--------------------------------*- C++ -*----------------------------------*\
| =========                 |                                                 |
| \\      /  F ield         | OpenFOAM: The Open Source CFD Toolbox           |
|  \\    /   O peration     | Version:  1.7.1                                 |
|   \\  /    A nd           | Web:      www.OpenFOAM.com                      |
|    \\/     M anipulation  |                                                 |
\*---------------------------------------------------------------------------*/
FoamFile
{
    version     2.0;
    format      ascii;
    class       dictionary;
    location    "system";
    object      controlDict;
}
// * * * * * * * * * * * * * * * * * * * * * * * * * * * * * * * * * * * * //

application     interFoam;

startFrom       latestTime;

startTime       0;

stopAt          endTime;

endTime         2;

deltaT          0.0005;
writeControl    adjustableRunTime;

writeInterval   0.001;

purgeWrite      0;

writeFormat     ascii;

writePrecision  6;

writeCompression compressed;

timeFormat      general;

timePrecision   6;

runTimeModifiable yes;

adjustTimeStep  yes;

maxCo           0.75;
maxAlphaCo      0.75;

maxDeltaT       1;

// ************************************************************************* //
```

Figure A.4: ControlDict file.

Figure A.5 shows the content in *fvSchemes* dictionary, where are defined the numerical schemes for derivative equations, among other terms. In ddtSchemes are defined the first and second time derivatives ($\delta/\delta t, \delta^2/\delta^2 t$), the gradient schemes (∇) in gradSchemes, the divergence ones ($\nabla\cdot$) in divSchemes, Laplacian (∇^2) in laplacianSchemes, the cell to face interpolations in interpolationSchemes, the gradient component normal to a cell in snGradSchemes, and finally in fluxRequired are defined the fields which need a flux generation.

```
/*--------------------------------*- C++ -*----------------------------------*\
| =========                 |                                                 |
| \\      /  F ield         | OpenFOAM: The Open Source CFD Toolbox           |
|  \\    /   O peration     | Version:  1.7.1                                 |
|   \\  /    A nd           | Web:      www.OpenFOAM.com                      |
|    \\/     M anipulation  |                                                 |
\*---------------------------------------------------------------------------*/
FoamFile
{
    version     2.0;
    format      ascii;
    class       dictionary;
    location    "system";
    object      fvSchemes;
}
// * * * * * * * * * * * * * * * * * * * * * * * * * * * * * * * * * * * * //

ddtSchemes
{
    default         Euler;
}

gradSchemes
{
    default         Gauss linear;
}

divSchemes
{
    div(rhoPhi,U)  Gauss limitedLinearV 1;
    div(phi,alpha)  Gauss vanLeer;
    div(phirb,alpha) Gauss interfaceCompression;
    div(((rho*nuEff)*dev2(T(grad(U))))) Gauss linear;
}

laplacianSchemes
{
    default         Gauss linear corrected;
}

interpolationSchemes
{
    default         linear;
}

snGradSchemes
{
    default         corrected;
}

fluxRequired
{
    default          no;
    p_rgh;
    pcorr;
    alpha.water;
}
// ************************************************************************* //
```

Figure A.5: FvSchemes file.

The fvSolution file (Figure A.6) controls for each particular field the equation solvers, tolerances, and algorithms. The term PIMPLE is referred to the algorithm used for the simulations.

```
/*--------------------------------*- C++ -*----------------------------------*\
| =========                 |                                                 |
| \\      /  F ield         | OpenFOAM: The Open Source CFD Toolbox           |
|  \\    /   O peration     | Version:  1.7.1                                 |
|   \\  /    A nd           | Web:      www.OpenFOAM.com                      |
|    \\/     M anipulation  |                                                 |
\*---------------------------------------------------------------------------*/
FoamFile
{
    version     2.0;
    format      ascii;
    class       dictionary;
    location    "system";
    object      fvSolution;
}
// * * * * * * * * * * * * * * * * * * * * * * * * * * * * * * * * * * * * * //

solvers
{
   "alpha.water.*"
    {
        nAlphaCorr      1;
        nAlphaSubCycles 2;
        cAlpha          1;

        MULESCorr       yes;
        nLimiterIter    5;
        solver          smoothSolver;
        smoother        symGaussSeidel;
        tolerance       1e-8;
        relTol          0;
    }

    "pcorr.*"
    {
        solver          PCG;
        preconditioner  DIC;
        tolerance       1e-10;
        relTol          0;
    }

    p_rgh
    {
        solver          PCG;
        preconditioner  DIC;
        tolerance       1e-07;
        relTol          0.05;
    }

    p_rghFinal
    {
        solver          GAMG;
        tolerance       1e-08;
        relTol          0.0;
        smoother        GaussSeidel;
        cacheAgglomeration off;
        nCellsInCoarsestLevel 20;
        agglomerator    faceAreaPair;
        mergeLevels     1;
    }

    U
    {
        solver          PBiCG;
        preconditioner  DILU;
        tolerance       1e-06;
        relTol          0;
    }
    UFinal
    {
        $U;
    }
}

PIMPLE
{
       momemntumPredictor      no;
       nOuterCorrectors        1;
       nCorrectors             3;
       nNonOrthogonalCorrectors 0;
}

// ************************************************************************* //
```

Figure A.6: FvSolution file.

Figure A.7 is a captures of the file SetFields. This is used to define a characteristic fluid volume inside the geometry generated. In the case showed it has been set $\alpha = 1$ inside the vessel except the top of the cylinder which is defined as air, in order to represent the free surface in contact with the atmosphere.

```
/*--------------------------------*- C++ -*----------------------------------*\
| =========                 |                                                 |
| \\      /  F ield         | OpenFOAM: The Open Source CFD Toolbox           |
|  \\    /   O peration     | Version:  1.7.1                                 |
|   \\  /    A nd           | Web:      www.OpenFOAM.com                      |
|    \\/     M anipulation  |                                                 |
\*---------------------------------------------------------------------------*/
FoamFile
{
    version     2.0;
    format      ascii;
    class       dictionary;
    location    "system";
    object      setFieldsDict;
}
// * * * * * * * * * * * * * * * * * * * * * * * * * * * * * * * * * * * * * //

defaultFieldValues
(
    volScalarFieldValue alpha.water 1
);

regions
(
    cylinderToCell
    {
        p1 (0 0 0.021); // Edit box bounds as required
        p2 (0 0 0.022);
        radius 0.0035;
        fieldValues
        (
            volScalarFieldValue alpha.water 0
        );
    }
);


// ************************************************************************* //
```

Figure A.7: SetFields file.

Finally, one of the most important files inside system folder is the *blockMeshDict*, which is responsible of the mesh generation. The principle behind this file is to decompose the geometry's domain into a set of 1 or more three dimensional, hexahedral blocks. The edges of the blocks can be straight lines, arcs or splines, and besides the mesh is specified as a number of cells in each direction of the block. But the reality is that it was found a macro for cylinder mesh [17], which defining some specific parameters is able to automatically generate the *blockMeshDict* giving much more freedom to modify the geometry and mesh of the problem. So, this m4 file can be seen in figure A.8:

```
/*--------------------------------*- C++ -*----------------------------------*\
| =========                 |                                                 |
| \\      /  F ield         | OpenFOAM: The Open Source CFD Toolbox           |
|  \\    /   O peration     |                                                 |
|   \\  /    A nd           | Copyright (C) 2016 Ehsan Madadi-Kandjani        |
|    \\/     M anipulation  |                                                 |
\*---------------------------------------------------------------------------*/
FoamFile
{
    version     2.0;
    `format'      ascii;
    class       dictionary;
    object      blockMeshDict;
}
// * * * * * * * * * * * * * * * * * * * * * * * * * * * * * * * * * * * * //
// General macros to create cylinder mesh

changecom(//)changequote([,])
define(calc, [esyscmd(perl -e 'use Math::Trig; print ($1)')])
define(VCOUNT, 0)
define(vlabel, [[// ]Vertex $1 = VCOUNT define($1, VCOUNT)define([VCOUNT], incr(VCOUNT))])

define(hex2D, hex ($1b $2b $3b $4b $1t $2t $3t $4t))
define(btQuad, ($1b $2b $2t $1t))
define(topQuad, ($1t $4t $3t $2t))
define(bottomQuad, ($1b $2b $3b $4b))

// * * * * * * * * * * * * * * * * * * * * * * * * * * * * * * * * * * * * //

convertToMeters 1;

// Inner square side half
define(s, 0.00037)

// Inner square side curvature
define(sc, 0.0005)

// cylinder radius
define(r, 0.0035)

// Height of cylinder
define(z, 0.022)

// Base z
define(Zb, 0)

// Outlet z
define(Zt, calc(Zb + z))




// cylinder radius
define(r, 0.0035)

// Height of cylinder
define(z, 0.022)

// Base z
define(Zb, 0)

// Outlet z
define(Zt, calc(Zb + z))

// Number of cells at inner square
define(Ns, 15)

// Number of cells between inner square and circle
define(Ni, 32)

// Number of cells in the cylinder height
define(Nz, 130)

// * * * * * * * * * * * * * * * * * * * * * * * * * * * * * * * * * * * * //

define(vert, (x$1$2 y$1$2 $3))
define(evert, (ex$1$2 ey$1$2 $3))

// 45 degree points angle
define(a0, -45)
define(a1, -135)
define(a2, 135)
define(a3, 45)

// Half of 45 degree points angle
define(ea0, 0)
define(ea1, -90)
define(ea2, 180)
define(ea3, 90)

define(ca0, calc(cos((pi/180)*a0)))
define(ca1, calc(cos((pi/180)*a1)))
define(ca2, calc(cos((pi/180)*a2)))
define(ca3, calc(cos((pi/180)*a3)))

define(sa0, calc(sin((pi/180)*a0)))
define(sa1, calc(sin((pi/180)*a1)))
define(sa2, calc(sin((pi/180)*a2)))
define(sa3, calc(sin((pi/180)*a3)))
```

```
define(cea0, calc(cos((pi/180)*ea0)))
define(cea1, calc(cos((pi/180)*ea1)))
define(cea2, calc(cos((pi/180)*ea2)))
define(cea3, calc(cos((pi/180)*ea3)))

define(sea0, calc(sin((pi/180)*ea0)))
define(sea1, calc(sin((pi/180)*ea1)))
define(sea2, calc(sin((pi/180)*ea2)))
define(sea3, calc(sin((pi/180)*ea3)))

// Inner square x and y position

// x
define(x00, s)
define(x01, calc(-1.0*s))
define(x02, calc(-1.0*s))
define(x03, s)

// y
define(y00, calc(-1.0*s))
define(y01, calc(-1.0*s))
define(y02, s)
define(y03, s)

// Circle x and y positions

// x
define(xl0, calc(r*ca0))
define(xl1, calc(r*ca1))
define(xl2, calc(r*ca2))
define(xl3, calc(r*ca3))

// y
define(yl0, calc(r*sa0))
define(yl1, calc(r*sa1))
define(yl2, calc(r*sa2))
define(yl3, calc(r*sa3))

// Inner square x and y position middle curvatures

// x
define(ex00, sc)
define(ex01, 0)
define(ex02, calc(-1.0*sc))
define(ex03, 0)




    // y
    define(ey00, 0)
    define(ey01, calc(-1.0*sc))
    define(ey02, 0)
    define(ey03, sc)

    // Circle x and y positions middle curvatures

    // x
    define(exl0, calc(r*cea0))
    define(exl1, calc(r*cea1))
    define(exl2, calc(r*cea2))
    define(exl3, calc(r*cea3))

    // y
    define(eyl0, calc(r*sea0))
    define(eyl1, calc(r*sea1))
    define(eyl2, calc(r*sea2))
    define(eyl3, calc(r*sea3))

    // * * * * * * * * * * * * * * * * * * * * * * * * * * * * * * * * * * * * * * * * * * * * * * * * * //

    vertices
    (
        vert(0, 0, Zb) vlabel(s0b)
        vert(0, 1, Zb) vlabel(s1b)
        vert(0, 2, Zb) vlabel(s2b)
        vert(0, 3, Zb) vlabel(s3b)

        vert(1, 0, Zb) vlabel(r0b)
        vert(1, 1, Zb) vlabel(r1b)
        vert(1, 2, Zb) vlabel(r2b)
        vert(1, 3, Zb) vlabel(r3b)

        vert(0, 0, Zt) vlabel(s0t)
        vert(0, 1, Zt) vlabel(s1t)
        vert(0, 2, Zt) vlabel(s2t)
        vert(0, 3, Zt) vlabel(s3t)

        vert(1, 0, Zt) vlabel(r0t)
        vert(1, 1, Zt) vlabel(r1t)
        vert(1, 2, Zt) vlabel(r2t)
        vert(1, 3, Zt) vlabel(r3t)
    );
```

```
blocks
(
    //block0
    hex2D(s1, s0, s3, s2)
    square
    (Ns Ns Nz)
    simpleGrading (1 1 2)

    //block1
    hex2D(s0, r0, r3, s3)
    innerCircle
    (Ni Ns Nz)
    simpleGrading (1.25 1 2)

    //block2
    hex2D(s3, r3, r2, s2)
    innerCircle
    (Ni Ns Nz)
    simpleGrading (1.25 1 2)

    //block3
    hex2D(s2, r2, r1, s1)
    innerCircle
    (Ni Ns Nz)
    simpleGrading (1.25 1 2)

    //block4
    hex2D(s1, r1, r0, s0)
    innerCircle
    (Ni Ns Nz)
    simpleGrading (1.25 1 2)
);

edges
(
    //Circle edges
    arc r3b r0b evert(1, 0, Zb)
    arc r0b r1b evert(1, 1, Zb)
    arc r1b r2b evert(1, 2, Zb)
    arc r2b r3b evert(1, 3, Zb)

    //Circle edges
    arc r3t r0t evert(1, 0, Zt)
    arc r0t r1t evert(1, 1, Zt)
    arc r1t r2t evert(1, 2, Zt)
    arc r2t r3t evert(1, 3, Zt)



       arc s3b s0b evert(0, 0, Zb)
       arc s0b s1b evert(0, 1, Zb)
       arc s1b s2b evert(0, 2, Zb)
       arc s2b s3b evert(0, 3, Zb)

       arc s3t s0t evert(0, 0, Zt)
       arc s0t s1t evert(0, 1, Zt)
       arc s1t s2t evert(0, 2, Zt)
       arc s2t s3t evert(0, 3, Zt)

   );

   patches
   (
       wall fixedWall
       (
           btQuad(r0, r3)
           btQuad(r1, r0)
           btQuad(r2, r1)
           btQuad(r3, r2)
       bottomQuad(s3, r3, r0, s0)
           bottomQuad(s2, r2, r3, s3)
           bottomQuad(s1, r1, r2, s2)
           bottomQuad(s0, r0, r1, s1)
       )

       patch inlet
       (
           bottomQuad(s3, s0, s1, s2)
       )

       patch outlet
       (
           topQuad(s3, s0, s1, s2)
           topQuad(s3, r3, r0, s0)
           topQuad(s2, r2, r3, s3)
           topQuad(s1, r1, r2, s2)
           topQuad(s0, r0, r1, s1)
       )
   );

   mergePatchPairs
   (
   );
```

Figure A.8: BlockMeshDict macro file.

A.1.3. 0 folder

Inside 0 folder there are three different files, one for each field of interest: *alpha* (Figure A.9), *p_ rgh* (Figure A.10) and *U* (Figure A.11). All files in this folder have the same format. First, the dimensions are defined as it is explained at the beginning of the appendix. Then the internalField parameter describes the initial value of the internal fluid and boundaryField determines the boundary conditions of each surface of the geometry. This geometry is divided in three parts: inlet (air entrance), outlet (free surface) and fixed walls (solid surfaces of the vessel). So, in the following figures can be appreciated the different boundary and initial conditions chosen for each field depending on the geometry part.

```
/*--------------------------------*- C++ -*----------------------------------*\
| =========                 |                                                 |
| \\      /  F ield         | OpenFOAM: The Open Source CFD Toolbox           |
|  \\    /   O peration     | Version:  1.7.x                                 |
|   \\  /    A nd           | Web:      www.OpenFOAM.com                      |
|    \\/     M anipulation  |                                                 |
\*---------------------------------------------------------------------------*/
FoamFile
{
    version     2.0;
    format      ascii;
    class       volScalarField;
    location    "0";
    object      alpha.water.orig;
}
// * * * * * * * * * * * * * * * * * * * * * * * * * * * * * * * * * * * * * //

dimensions      [0 0 0 0 0 0 0];

internalField   uniform 1;

boundaryField
{
    fixedWall
    {
        type            constantAlphaContactAngle;
        theta0          25;
        limit           gradient;
        value           uniform 1;
    }
    inlet
    {
        type            inletOutlet;
        inletValue      uniform 0;
        value           uniform 0;
    }

    outlet
    {
        type            inletOutlet;
        inletValue      uniform 0;
        value           uniform 0;
    }

}
// ************************************************************************* //
```

Figure A.9: Alpha file.

```
/*--------------------------------*- C++ -*----------------------------------*\
| =========                 |                                                 |
| \\      /  F ield         | OpenFOAM: The Open Source CFD Toolbox           |
|  \\    /   O peration     | Version:  1.7.x                                 |
|   \\  /    A nd           | Web:      www.OpenFOAM.com                      |
|    \\/     M anipulation  |                                                 |
\*---------------------------------------------------------------------------*/
FoamFile
{
    version     2.0;
    format      ascii;
    class       volScalarField;
    location    "0";
    object      p_rgh;
}
// * * * * * * * * * * * * * * * * * * * * * * * * * * * * * * * * * * * * * //

dimensions      [1 -1 -2 0 0 0 0];

internalField   uniform 0;

boundaryField
{
    fixedWall
    {
        type            fixedFluxPressure;
        gradient        uniform 0;
        rho             rho;
        value           uniform 0;
    }
    inlet
    {
        type            fixedFluxPressure;
        value           uniform 0;
    }

    outlet
    {
        type            totalPressure;
        p0              uniform 0;
        U               U;
        phi             phi;
        rho             rho;
        psi             none;
        gamma           1;
        value           uniform 0;
    }
}
// ************************************************************************* //
```

Figure A.10: Pressure file.

```
/*--------------------------------*- C++ -*----------------------------------*\
| =========                 |                                                 |
| \\      /  F ield         | OpenFOAM: The Open Source CFD Toolbox           |
|  \\    /   O peration     | Version:  1.7.x                                 |
|   \\  /    A nd           | Web:      www.OpenFOAM.com                      |
|    \\/     M anipulation  |                                                 |
\*---------------------------------------------------------------------------*/
FoamFile
{
    version     2.0;
    format      ascii;
    class       volVectorField;
    location    "0";
    object      U;
}
// * * * * * * * * * * * * * * * * * * * * * * * * * * * * * * * * * * * * * //

dimensions      [0 1 -1 0 0 0 0];

internalField   uniform (0 0 0);

boundaryField
{
    fixedWall
    {
        type            fixedValue;
        value           uniform (0 0 0);
    }
    inlet
    {
        type            fixedValue;
        value           uniform (0 0 0.06);
    }
    outlet
    {
        type            inletOutlet;
        inletValue      uniform (0 0 0);
        value           uniform (0 0 0);
    }
}

// ************************************************************************* //
```

Figure A.11: Velocity file.

APPENDIX B. MESH GENERATION

First of all, it was attempted to generate the mesh with GMSH. This software is a free 3D finite element mesh generator that provides a fast meshing tool with parametric input, although the most important capability is the advanced visualization that OpenFOAM doesn't provides. The modules used in GMSH were: geometry and mesh, as they were the only ones needed for the grid generation.

Below, it can be seen the first meshed volume test. In order to simplify the complexity of the figure, it was created a parallelepiped volume. The figure B.1 is composed by a top view, where it can be appreciated a more refined mesh in the centre circle (gas injector) that goes degrading to the end; a front view that shows the layers of the grid in the vertical axis; and finally the total 3D mesh of the figure.

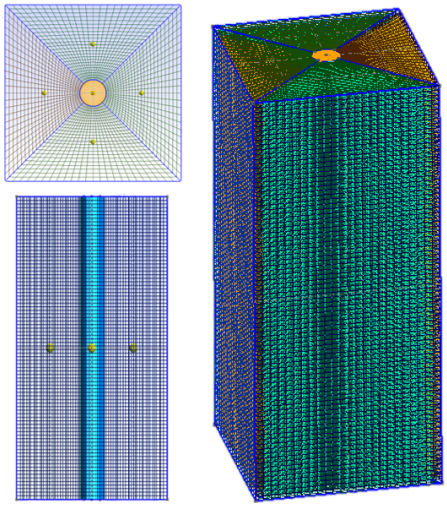

Figure B.1: Different views of the parallelepiped volume meshed.

However, it was also tried to generate a cylindrical volume and its mesh. This decision was made especially because the right angles of the corners would probably give problems for the computations just on the basis that they are harsh geometry. For this reason, it was created another GMSH test with some improvements such a cylindrical volume in which the grid would be placed, and a vertical degradation of the grid to increase the refinement in the critical parts of the vessel mentioned before. In the figure B.2 can be appreciated a zoom of the gas injection area mesh, besides the typical views.

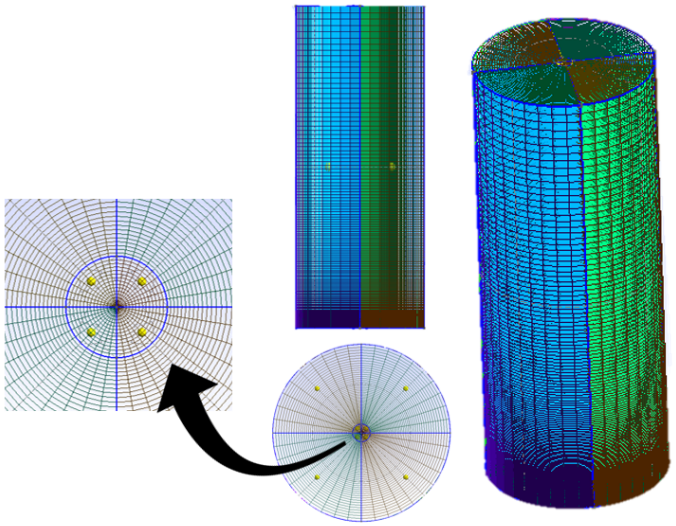

Figure B.2: Views of the mesh in the cylindrical volume.

Despite the design was successful, once the mesh was tested in the simulation performed by OpenFOAM, some deficiencies were found in the fluid behaviour. After some simulations it was detected that the deficiencies were caused due to the format conversion from GMSH to OpenFOAM. Apparently, the gas was injected by four different sites from the injection area, which coincided with the fact that the cylinder was generated by rotating a rectangular surface four times. Therefore, it was deduced that the cylinder was split into four parts by mistake. The problem set out a new path concerning the mesh design. From this point, it was started the stage of mesh generation with the OpenFOAM, thus any possible format problem would be avoided.